HAL open science

Cholangiopathy and biliary fibrosis in Cyp2c70-deficient mice are fully reversed by ursodeoxycholic acid

Jan Freark de Boer, Hilde D de Vries, Anna Palmiotti, Rumei Li, Marwah Doestzada, Joanne A Hoogerland, Jingyuan Fu, Anouk M La Rose, Marit Westerterp, Niels L Mulder, et al.

To cite this version:

Jan Freark de Boer, Hilde D de Vries, Anna Palmiotti, Rumei Li, Marwah Doestzada, et al.. Cholangiopathy and biliary fibrosis in Cyp2c70-deficient mice are fully reversed by ursodeoxycholic acid. Cellular and Molecular Gastroenterology and Hepatology, 2021, 11 (4), pp.1045-1069. 10.1016/j.jcmgh.2020.12.004 . inserm-03177441

HAL Id: inserm-03177441

https://inserm.hal.science/inserm-03177441

Submitted on 23 Mar 2021

HAL is a multi-disciplinary open access archive for the deposit and dissemination of scientific research documents, whether they are published or not. The documents may come from teaching and research institutions in France or abroad, or from public or private research centers.

L'archive ouverte pluridisciplinaire **HAL**, est destinée au dépôt et à la diffusion de documents scientifiques de niveau recherche, publiés ou non, émanant des établissements d'enseignement et de recherche français ou étrangers, des laboratoires publics ou privés.

Distributed under a Creative Commons Attribution - NonCommercial - NoDerivatives 4.0 International License

cmgh
CELLULAR AND MOLECULAR GASTROENTEROLOGY AND HEPATOLOGY

ORIGINAL RESEARCH

Cholangiopathy and Biliary Fibrosis in Cyp2c70-Deficient Mice Are Fully Reversed by Ursodeoxycholic Acid

Jan Freark de Boer,[1,2] Hilde D. de Vries,[2,3] Anna Palmiotti,[1] Rumei Li,[1] Marwah Doestzada,[1,4] Joanne A. Hoogerland,[5] Jingyuan Fu,[1,4] Anouk M. La Rose,[1] Marit Westerterp,[1] Niels L. Mulder,[1] Milaine V. Hovingh,[1] Martijn Koehorst,[2] Niels J. Kloosterhuis,[1] Justina C. Wolters,[1] Vincent W. Bloks,[1] Joel T. Haas,[5] David Dombrowicz,[5] Bart Staels,[5] Bart van de Sluis,[1,6] and Folkert Kuipers[1,2]

[1]Department of Pediatrics, University of Groningen, University Medical Center Groningen, the Netherlands; [2]Department of Laboratory Medicine, University of Groningen, University Medical Center Groningen, Groningen, the Netherlands; [3]University of Groningen, Campus Fryslân, Leeuwarden, the Netherlands; [4]Department of Genetics University of Groningen, University Medical Center Groningen, Groningen, the Netherlands; [5]Univ. Lille, Inserm, CHU Lille, Institut Pasteur Lille, U1011-EGID, F-59000 Lille, France; and [6]iPSC/CRISPR Center Groningen, University of Groningen, University Medical Center Groningen, Groningen, the Netherlands

SUMMARY

We characterized *Cyp2c70*-deficient mice, possessing a human-like bile acid composition. While both sexes display transient neonatal cholestasis, only female mice develop considerable pathologic features with age. Treatment with the hydrophilic bile acid ursodeoxycholic acid reverses liver pathology in female *Cyp2c70*-deficient mice.

BACKGROUND AND AIMS: Bile acids (BAs) aid intestinal fat absorption and exert systemic actions by receptor-mediated signaling. BA receptors have been identified as drug targets for liver diseases. Yet, differences in BA metabolism between humans and mice hamper translation of pre-clinical outcomes. *Cyp2c70*-ablation in mice prevents synthesis of mouse/rat-specific muricholic acids (MCAs), but potential (patho)physiological consequences of their absence are unknown. We therefore assessed age- and gender-dependent effects of *Cyp2c70*-deficiency in mice.

METHODS: The consequences of *Cyp2c70*-deficiency were assessed in male and female mice at different ages.

RESULTS: *Cyp2c70*$^{-/-}$ mice were devoid of MCAs and showed high abundances of chenodeoxycholic and lithocholic acids. *Cyp2c70*-deficiency profoundly impacted microbiome composition. Bile flow and biliary BA secretion were normal in *Cyp2c70*$^{-/-}$ mice of both sexes. Yet, the pathophysiological consequences of *Cyp2c70*-deficiency differed considerably between sexes. Three-week old male *Cyp2c70*$^{-/-}$ mice showed high plasma BAs and transaminases, which spontaneously decreased thereafter to near-normal levels. Only mild ductular reactions were observed in male *Cyp2c70*$^{-/-}$ mice up to 8 months of age. In female *Cyp2c70*$^{-/-}$ mice, plasma BAs and transaminases remained substantially elevated with age, gut barrier function was impaired and bridging fibrosis was observed at advanced age. Addition of 0.1% ursodeoxycholic acid to the diet fully normalized hepatic and intestinal functions in female *Cyp2c70*$^{-/-}$ mice.

CONCLUSION: *Cyp2c70*$^{-/-}$ mice show transient neonatal cholestasis and develop cholangiopathic features that progress to bridging fibrosis in females only. These consequences of *Cyp2c70*-deficiency are restored by treatment with UDCA, indicating a role of BA hydrophobicity in disease development. *(Cell Mol Gastroenterol Hepatol 2021;11:1045–1069; https://doi.org/10.1016/j.jcmgh.2020.12.004)*

Keywords: Bile Acids; Liver; Humanized Mouse Model; Primary Biliary Cholangitis.

See editorial on page 1207.

Bile acids (BAs) are amphipathic molecules present in all vertebrates, but their chemical structures may differ between species.[1] BAs are synthesized in the liver from cholesterol and aid the absorption of lipid-soluble nutrients from the intestine. Moreover, BAs exert hormone-like functions in control of lipid and glucose metabolism and of immune responses via specialized receptors, including farnesoid X receptor (FXR) (NR1H4), vitamin D receptor (NR1I1), and Takeda G protein–coupled receptor 5 (TGR5).[2]

Humans synthesize 2 primary BAs, cholic acid (CA) and chenodeoxycholic acid (CDCA). Specific intestinal bacteria can metabolize these BAs to generate the secondary species deoxycholic acid (DCA) and lithocholic acid (LCA), respectively. In mice, CDCA is efficiently converted into muricholic acids (MCAs), which constitute 30%–40% of the murine BA

Abbreviations used in this paper: **BA, bile acid; CA, cholic acid; CDCA, chenodeoxycholic acid; DCA, deoxycholic acid; DNL, de novo lipogenesis; ER, endoplasmic reticulum; FDR, false discovery rate; FXR, farnesoid X receptor; LCA, lithocholic acid; LDL, low-density lipoprotein; LDLR, low-density lipoprotein receptor; MCA, muricholic acid; mRNA, messenger RNA; PBC, primary biliary cholangitis; PBS, phosphate-buffered saline; UDCA, ursodeoxycholic acid; WT, wild-type.**

Most current article

© 2021 The Authors. Published by Elsevier Inc. on behalf of the AGA Institute. This is an open access article under the CC BY-NC-ND license (http://creativecommons.org/licenses/by-nc-nd/4.0/).
2352-345X
https://doi.org/10.1016/j.jcmgh.2020.12.004

pool.[3] Recently, CYP2C70 was reported to be involved in the generation of MCAs in mice.[4] Using isotopically labeled tracers following acute hepatic inactivation of *Cyp2c70* in mice, we could demonstrate that CYP2C70 catalyzes the conversion of CDCA into αMCA as well as its subsequent conversion into βMCA.[5] In line with our data,[5] other studies have recently confirmed that deletion of *Cyp2c70* indeed leads to a complete absence of MCAs in mice.[6,7]

Given the highly divergent physicochemical properties of the various BA species, differences in BA metabolism between animal species obviously complicate translational research on the role of BAs in disease development. Accumulation of BAs contributes to liver damage in obstructive cholestasis, progressive familial intrahepatic cholestasis, primary sclerosing cholangitis, and primary biliary cholangitis (PBC).[8,9] Human diseases involving BA-induced liver damage are difficult to mimic in mouse models, because of the aforementioned high abundance of MCAs in the murine BA pool.[3] These trihydroxylated BAs are very hydrophilic,[10] have a high critical micellar concentration, and possess poor lipid-solubilizing properties. Like ursodeoxycholic acid (UDCA), which is used in treatment of cholestatic liver diseases like PBC, MCAs do not cause cell damage and can even reduce cytotoxic effects of more hydrophobic BAs.[11]

The BA receptors FXR and TGR5 have been identified as bona fide drug targets for the treatment of metabolic and cholestatic liver diseases, including nonalcoholic fatty liver disease[12,13] and PBC.[14] Furthermore, these receptors play important roles in BA, glucose, lipid, and cholesterol metabolism.[15] The potency to activate FXR and TGR5, however, differs substantially between BA species. CDCA is the most potent endogenous FXR agonist,[16] while MCAs act oppositely and actually inhibit FXR activation.[17] In general, more hydrophobic BAs are also more potent agonists of TGR5.[18] Hence, owing to the efficient conversion of CDCA into MCAs in mice, the intrinsic potency of the circulating BA pool to activate these receptors differs substantially between mice and humans. Furthermore, metabolic conditions or (pharmacological) interventions that impact BA pool composition may differentially affect BA-mediated signaling pathways in mice and men.[5]

The recent discovery that CYP2C70 catalyzes the conversion of CDCA into MCAs in mice[4–7] paved the way for the generation of mouse models with a more human-like BA profile to study BA-related liver diseases, as well as the impact of BAs and pharmacological agents that target their signaling pathways on metabolic diseases.[19] However, the (patho)physiological consequences of the absence of MCAs in mice are still unexplored. Therefore, we assessed the effects of the human-like BA pool in *Cyp2c70*-deficient mice on liver and intestine (ie, the organs that constitute the enterohepatic circulation). Age and sex were included as variables in this study because human infants often experience a transient period of neonatal cholestasis with elevated plasma BAs, while some liver diseases that develop at more advanced ages display a sex bias, such as PBC[20] and nonalcoholic fatty liver disease.[21] We found that male *Cyp2c70*-deficient mice displayed transient liver dysfunction at weaning, which gradually improved with age, while liver pathology worsened and actually progressed to bridging fibrosis in female *Cyp2c70*-deficient mice at advanced age. Intriguingly, aberrations in liver function in *Cyp2c70*-deficient mice were fully restored by increasing the hydrophilicity of the BA pool by treatment with UDCA.

Results

Generation of Cyp2c70-Deficient Mice

Targeted inactivation of *Cyp2c70* yielded 3 mouse lines with mutations resulting in the introduction of an early stop codon in exon 1 (Figure 1*A*). Adult mice from all 3 *Cyp2c70*$^{-/-}$ lines displayed similar biliary BA compositions with a complete absence of MCAs (Figure 1*B*). Biliary BA profiles of *Cyp2c70*$^{+/-}$ mice were only performed for mice from the breeding lines containing the 11 nucleotide deletion or the 2 nucleotide insertion in the *Cyp2c70* gene and were very similar to their wild-type (WT) littermates. The breeding line with an 11 nucleotide deletion was used for further characterization of the (patho)physiological consequences of this human-like BA pool composition in mice. Absence of CYP2C70 protein in the livers of *Cyp2c70*$^{-/-}$ mice was confirmed by targeted proteomics (Figure 1*C*). *Cyp2c70*$^{-/-}$ mice were born in the expected Mendelian ratio (Figure 1*D*), but some *Cyp2c70*-deficient mice died shortly after weaning when pups were weaned at 3 weeks of age. This could be prevented by postponing weaning until the age of 4 weeks.

Cyp2c70$^{-/-}$ Mice Show Features of Neonatal Cholestasis

To evaluate potential early effects of *Cyp2c70* deficiency, we sacrificed mice at the age of 3 weeks and examined plasma and hepatic parameters as well as liver histology. Body weights did not differ between WT and *Cyp2c70*$^{-/-}$ mice (Figure 2*A*), but liver sizes were increased in male as well as female mice lacking *Cyp2c70* at this age (Figure 2*B*). Plasma transaminases were strongly elevated in young *Cyp2c70*$^{-/-}$ mice of both sexes (Figure 2*C*), as were total plasma BA levels (Figure 2*D*, inserts). *Cyp2c70*$^{-/-}$ mice of both sexes showed high abundances of (tauro-)CDCA in plasma (Figure 2*D*). Likely due to ingestion of exogenous BAs via milk from their heterozygous mothers or consumption of feces from mother and littermates, low levels of MCAs could be detected in these young *Cyp2c70*$^{-/-}$ mice. Hepatic gene expression analysis revealed that expression of *Fxr* was reduced in male and female *Cyp2c70*$^{-/-}$ mice, whereas expression of its target genes *Shp* (*Nr0b2*) and *Bsep* (*Abcb11*) was not significantly altered (Figure 2*E*). Nonetheless, robust decreases in hepatic expression of *Cyp7a1* and *Cyp8b1* indicate reduced BA synthesis in the *Cyp2c70*$^{-/-}$ animals (Figure 2*E*). A profibrotic gene expression pattern with increased *collagen type 1a1* (*Col1a1*) and tissue inhibitor of metalloproteinase (*Timp1*) was evident (Figure 2*E*), but histology revealed only mild collagen deposition in the livers of *Cyp2c70*$^{-/-}$ mice at this age (Figure 2*F*). Modest cholangiocyte proliferation appeared to be present, as evidenced by slightly increased *Krt19* gene expression and modestly higher numbers CK19-positive cells in the livers of

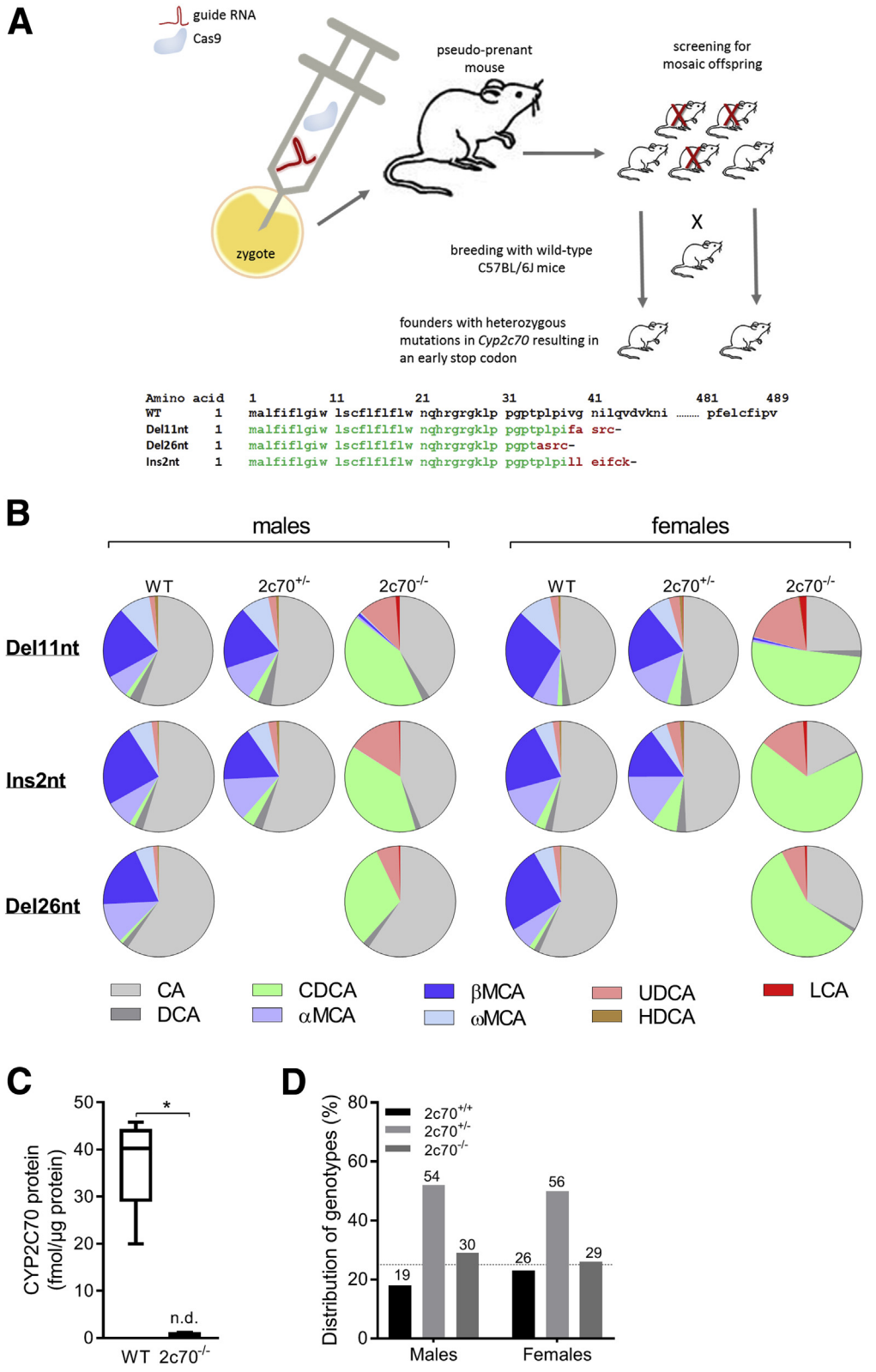

Figure 1. *Cyp2c70*-deficient mice are born in the normal Mendelian ratio. (*A*) Schematic representation of the generation of *Cyp2c70*$^{-/-}$ mice, yielding 3 different breeding lines. (*B*) Biliary BA composition in *Cyp2c70*$^{-/-}$ mouse lines with an 11 nucleotide deletion (Del11nt), a 2 nucleotide insertion (Ins2nt) and a 26 nucleotide deletion (Del26nt) in exon 1 of the *Cyp2c70* gene (n = 4–12 mice/group). (*C*) Hepatic CYP2C70-protein content, measured in mice with the 11 nucleotide deletion in the *Cyp2c70* gene sequence. (*D*) Genetic distribution of pups that were weaned at 4 weeks of age (numbers represent the total number of mice of the indicated gender and genotype that were weaned). * $P < .05$ between groups. 2c70$^{-/-}$, Cyp2c70$^{-/-}$. HDCA, hyodeoxycholic acid.

Cyp2c70$^{-/-}$ mice compared with WT littermates (Figure 2*E* and *F*). Hepatic expression of the macrophage marker *Cd68* as well as *Mcp-1* (*Ccl2*) and *Tnfα* were elevated in male and female *Cyp2c70*$^{-/-}$ mice (Figure 2*E*), indicating that inflammatory pathways were activated. Taken together, several characteristics of "neonatal cholestasis" were evident in 3-week-old *Cyp2c70*$^{-/-}$ mice, with no overt differences between male and female mice.

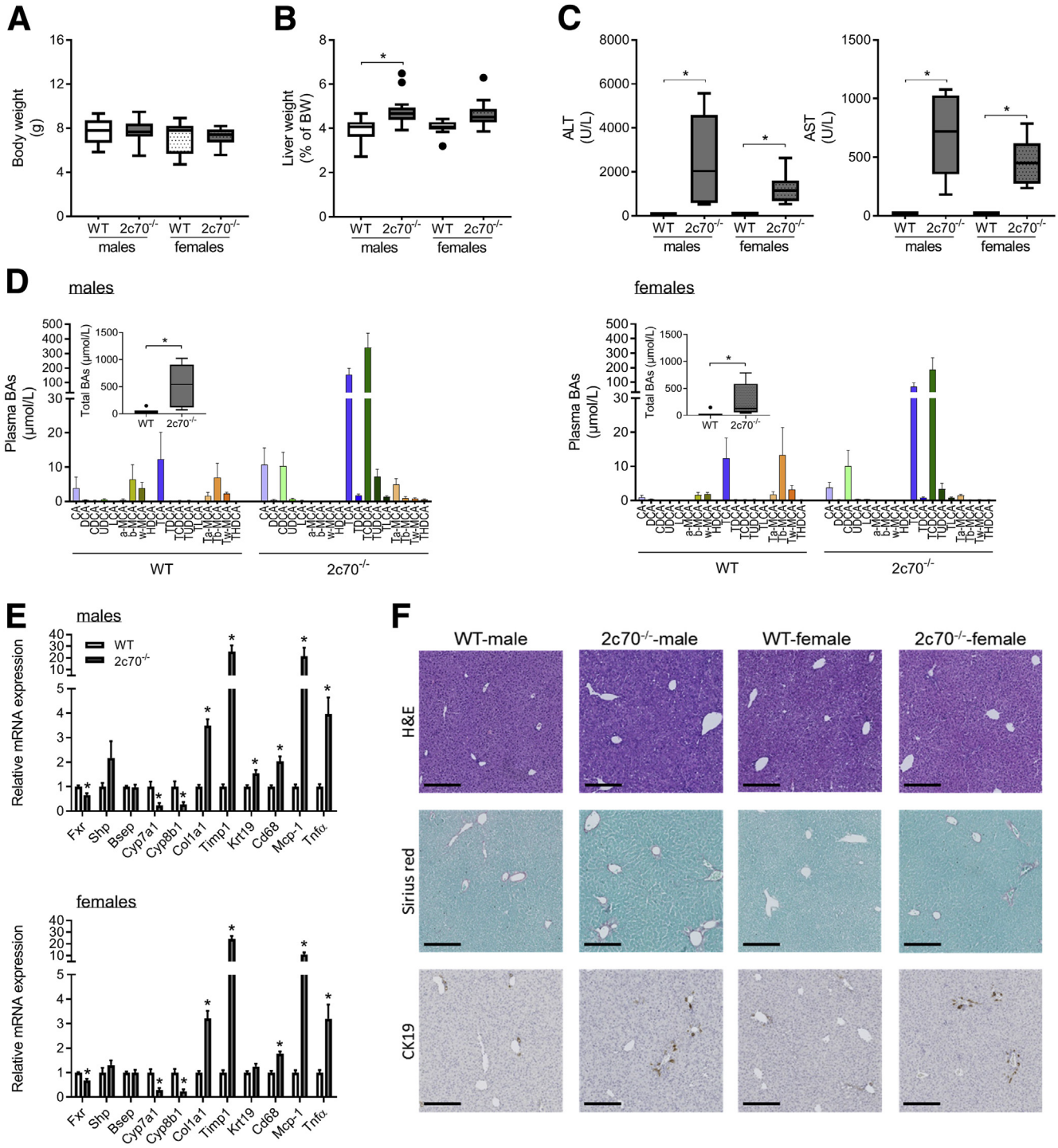

Figure 2. Young *Cyp2c70*-deficient mice show features of cholestasis. *Cyp2c70*$^{-/-}$ mice and WT littermates were sacrificed at the age of 3 weeks and characterized. (*A*) Body weights. (*B*) Liver weights. (*C*) Plasma transaminases. (*D*) Plasma BA profiles and total BA levels (inserts). (*E*) Hepatic mRNA expression. (*F*) Liver histology (black bars represent 200 μm). * $P < .05$ between groups (panels *A* and *B*, n = 6–21 mice/group; panels *C–F*, n = 6–8 randomly selected mice/group). ALT, alanine aminotransferase; AST, aspartate aminotransferase.

Characterization of BA Profiles in 12-Week-Old Cyp2c70$^{-/-}$ *Mice*

Body weight and food intake were not affected by absence of CYP2C70 in 12-week-old, young adult male and female mice (Table 1). These individually housed *Cyp2c70*$^{-/-}$ mice were completely devoid of α, β, and ω MCAs (Figure 3*A* and *B*). Instead, substantial amounts of CDCA were present. In contrast to their WT littermates,

Table 1. Characteristics of 12-Week-Old Cyp2c70$^{-/-}$ Mice

	Male mice		Female mice	
	WT (n = 12)	2c70$^{-/-}$ (n = 12)	WT (n = 7)	2c70$^{-/-}$ (n = 10)
Body weight, g	25.2 (24.5–25.6)	25.3 (24.4–26.3)	21.4 (20.7–23.4)	22.1 (21.8–22.4)
Food intake, g/d	4.4 (4.2–4.5)	4.8 (4.3–4.9)	4.0 (3.7–4.3)	3.7 (3.6–3.9)
Plasma				
Total cholesterol, mmol/L	2.4 (2.3–2.5)	2.4 (2.2–2.5)	1.9 (1.8–2.3)	2.3 (2.2–2.5)[a]
Free cholesterol, mmol/L	0.73 (0.69–0.75)	0.80 (0.74–0.83)	0.67 (0.63–0.70)	0.66 (0.59–0.78)
Cholesteryl ester, mmol/L	1.6 (1.6–1.8)	1.6 (1.5–1.7)	1.3 (1.2–1.5)	1.6 (1.5–1.8)[a]
Triglycerides, mmol/L	0.54 (0.39–0.69)	0.48 (0.29–0.72)	0.34 (0.29–0.51)	0.34 (0.26–0.50)
Free fatty acids, mmol/L	0.41 (0.36–1.2)	0.41 (0.31–0.59)	0.67 (0.32–0.81)	0.61 (0.44–0.65)
Liver				
Total cholesterol, μmol/g	5.9 (5.5–6.1)	6.6 (6.4–6.8)[b]	5.2 (4.7–5.5)	5.6 (5.2–6.0)
Free cholesterol, μmol/g	4.9 (4.7–5.0)	5.3 (5.2–5.7)[b]	4.1 (3.8–4.2)	4.5 (4.3–4.9)[b]
Cholesteryl ester, μmol/g	0.95 (0.93–1.08)	1.24 (1.18–1.47)[b]	1.1 (0.8–1.4)	1.0 (0.8–1.3)
Triglycerides, μmol/g	18.8 (16.3–20.5)	15.9 (12.7–18.5)[a]	12.7 (10.2–18.3)	6.5 (5.3–7.4)[b]
Phospholipids, μmol/g	29 (28–30)	29 (27–32)	29.6 (27.6–31.3)	28.7 (27.2–30.9)

NOTE. Values are median (interquartile range).
WT, wild-type; 2c70$^{-/-}$, Cyp2c70$^{-/-}$.
[a]$P < .05$ vs WT of same gender
[b]$P < .01$ vs WT of same gender using the Mann-Whitney *U* test.

(tauro-)LCA was clearly present in *Cyp2c70*$^{-/-}$ mice. Owing to the inability to convert UDCA into βMCA,[4,5] the amounts of (tauro-)UDCA in the BA pool were increased upon *Cyp2c70* deficiency (Figures 1*B* and 3*A*). Female WT mice had a more hydrophilic BA pool compared with WT male mice (Figure 3*C*). As a result of the altered abundance of BA species, the hydrophobicity index of biliary BAs was substantially increased in male as well as in female mice lacking *Cyp2c70* (Figure 3*C*). Interestingly, owing to the stronger increase in the relative abundance of hydrophobic BA species in female *Cyp2c70*$^{-/-}$ mice compared with WT, the hydrophobicity index of biliary BAs did not differ between male and female mice lacking *Cyp2c70*. Compared with WT, total plasma BA levels were elevated in 12-week old Cyp2c70$^{-/-}$ mice of both sexes, but the increase was more pronounced in female mice (Figure 3*D*). Yet, plasma BA levels in the 12-week old *Cyp2c70*$^{-/-}$ mice were considerably lower than at 3 weeks of age. In *Cyp2c70*$^{-/-}$ mice of both sexes, the relative abundances of secondary BAs were reduced compared with WT, whereas *Cyp2c70* deficiency did not affect the fraction of unconjugated BAs in the blood (Figure 3*E* and *F*).

Altered Bile Composition and BA Synthesis in Young adult Cyp2c70$^{-/-}$ Mice

Bile formation and biliary lipid secretion is driven by biliary BA secretion. Gallbladder cannulations demonstrated that bile flow was unaffected in *Cyp2c70*$^{-/-}$ mice, showing that these mice were not cholestatic by definition (Figure 4*A*).[22] Biliary BA secretion was also not impacted by *Cyp2c70* ablation (Figure 4*B*), although it was higher in female mice compared with male mice. However, in line with the greater potential of the hydrophobic BAs to promote biliary lipid secretion (Figure 4*C* and *D*),[23] the ratios of phospholipids and cholesterol to BAs were markedly increased in *Cyp2c70*$^{-/-}$ mice (Figure 4*E* and *F*).

Compared with male mice, female mice excreted more BAs with the feces. *Cyp2c70* deficiency tended to reduce fecal BA excretion in female mice but not in male mice (Figure 5*A*). Because fecal BA loss is compensated by BA synthesis, these data indicate that BA synthesis is higher in female mice compared with male mice and reduced only in female mice upon *Cyp2c70* deficiency. Indeed, hepatic *Cyp7a1*, *Cyp8b1*, *Cyp27a1*, and *Cyp7b1* were more strongly reduced in female mice than in male mice in absence of *Cyp2c70* (Figure 5*B* and *C*). Ileal expression of *Fgf15*, the intestine-derived regulator of hepatic BA synthesis, was not altered in either sex.

To quantify the impact of *Cyp2c70* deficiency on BA metabolism in detail, cholic acid (CA) kinetics were studied by isotope dilution after an intravenous bolus of [24-^{13}C]-CA (Figure 5*D*–*I*). WT female mice had larger CA and total BA pool sizes compared with WT male mice (Figure 5*F* and *G*). In male mice, CA pool size was reduced, whereas total BA pool size was not significantly impacted by *Cyp2c70* deficiency (Figure 5*F* and *G*). The fractional turnover rate of CA tended to be lower, whereas CA synthesis was reduced by 40% in male *Cyp2c70*$^{-/-}$ mice (Figure 5*H* and *I*). In female *Cyp2c70*$^{-/-}$ mice, CA pool size was reduced by 70% compared with WT mice, whereas total BA pool size was decreased by 40% (Figure 5*F* and *G*). The fractional turnover of CA was strongly decreased in female *Cyp2c70*$^{-/-}$ mice compared with WT (Figure 5*H*), and it was synthesized at only ~10% of the rate in age-matched WT female mice (Figure 5*I*). Collectively, the impact of *Cyp2c70* deficiency on BA metabolism was clearly more pronounced in female mice than in male mice.

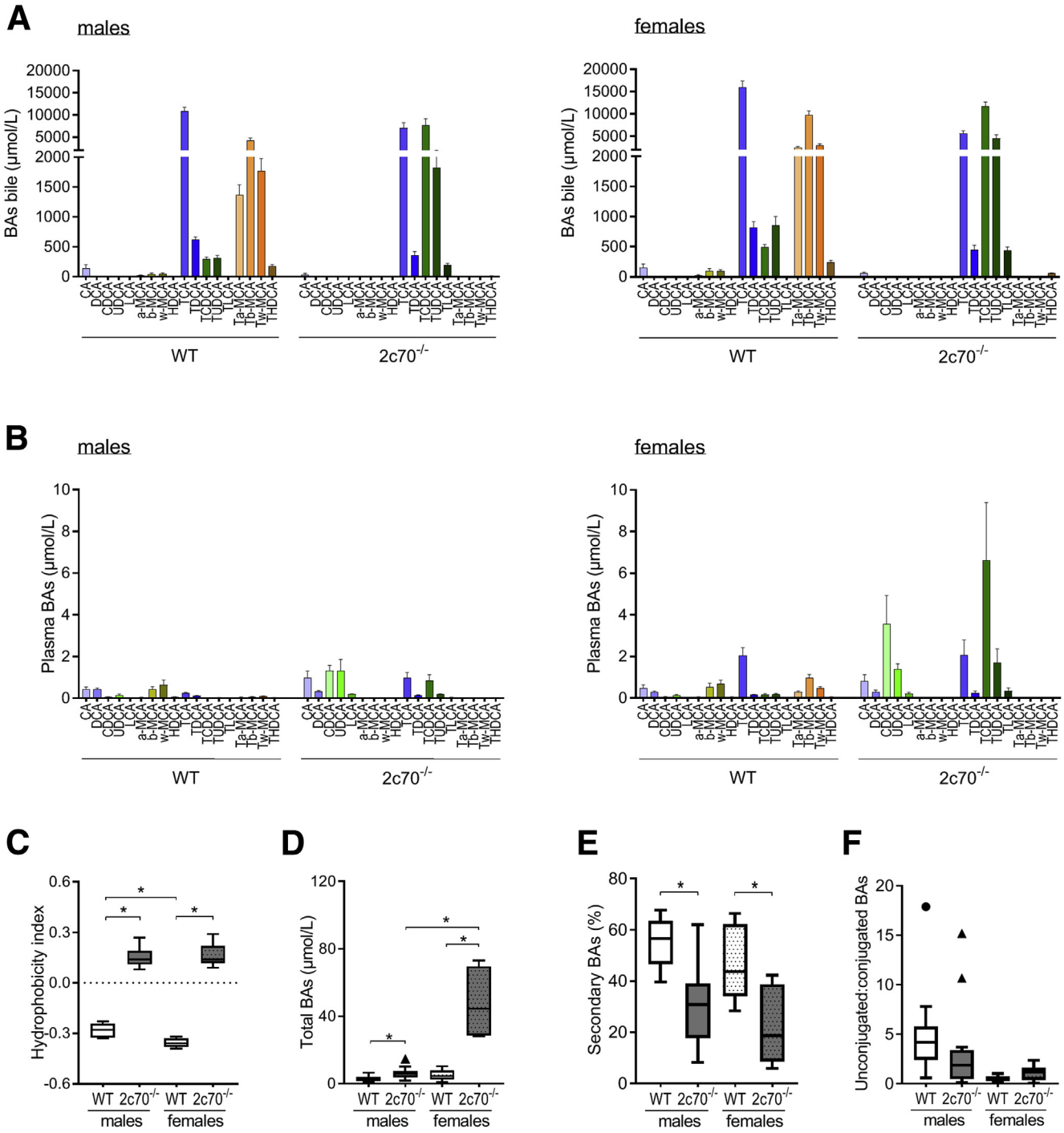

Figure 3. Young adult *Cyp2c70*-deficient mice possess a hydrophobic BA pool with substantial amounts of CDCA and LCA. *Cyp2c70*$^{-/-}$ mice and WT littermates were fed a standard rodent diet until the age of 12 weeks. BAs were quantified in (*A*) bile and (*B*) plasma. (*C*) Hydrophobicity index of biliary BAs. (*D*) Total plasma BA levels. (*E*) Percent secondary BAs in plasma. (*F*) Ratio unconjugated to conjugated BAs in plasma. *$P < .05$ between groups (n = 4–12 mice/group).

Because BA synthesis contributes significantly to whole body cholesterol turnover and BAs are important for fat absorption, plasma and hepatic lipids were analyzed (Table 1). *Cyp2c70*$^{-/-}$ mice of both genders displayed increased low-density lipoprotein (LDL) cholesterol levels compared with WT mice (Figure 6*A* and *B*). This was likely attributable to posttranscriptional downregulation of hepatic LDL receptor (LDLR) (Figure 6*C* and *D*), while cholesterol synthesis and intestinal fractional cholesterol absorption were unaffected in *Cyp2c70*$^{-/-}$ mice despite downregulation of *Npc1l1* in the small intestine (Figure 6*E*–*G*). Hepatic cholesterol content was slightly

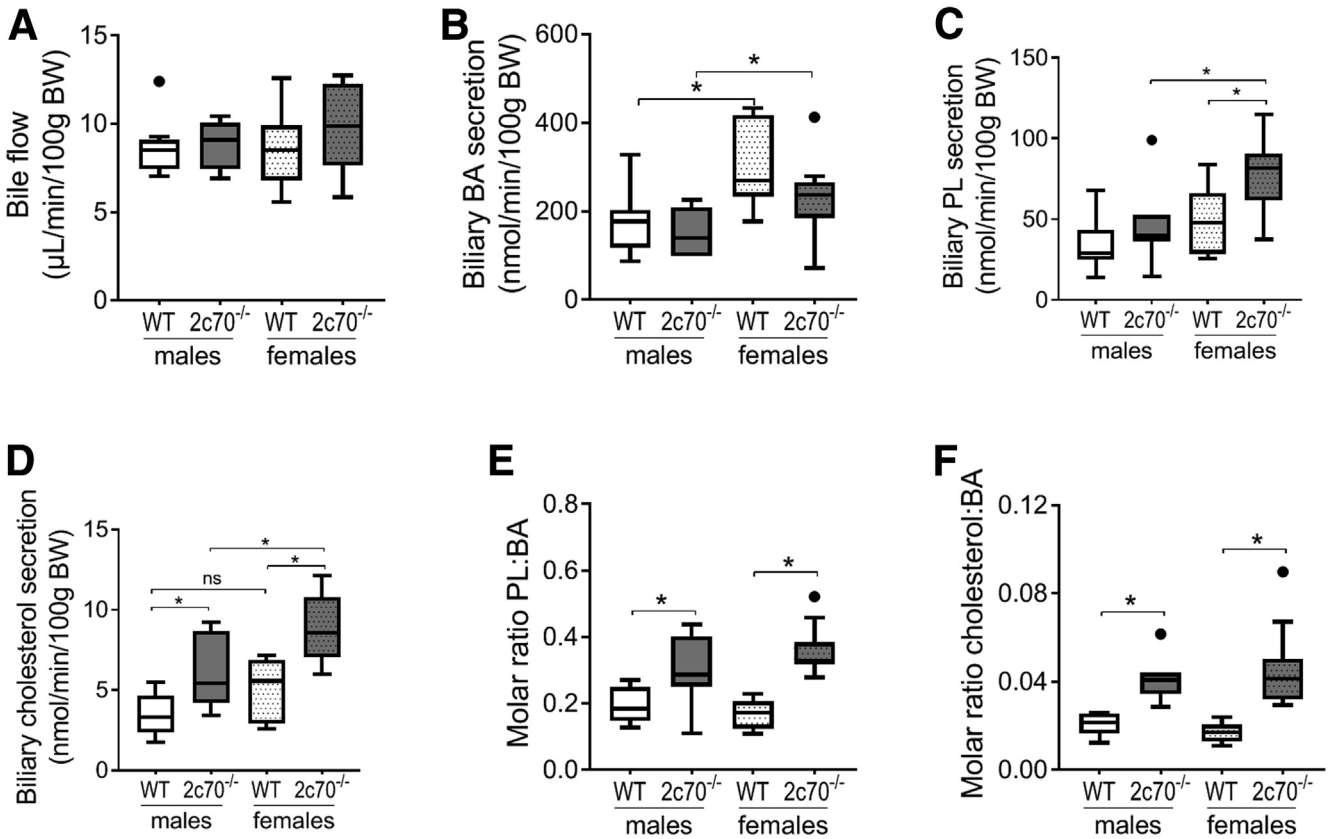

Figure 4. Hydrophobic BA pool in *Cyp2c70*-defient mice impacts bile formation. Gallbladders of 12-week-old *Cyp2c70*$^{-/-}$ mice and WT littermates were cannulated and parameters of bile formation were assessed. (*A*) Bile flow. (*B*) Biliary BA secretion rates. (C) Biliary phospholipid secretion rates. (*D*) Biliary cholesterol secretion rates. (*E*) Molar ratios of phospholipids to BAs. (*F*) Molar ratios of cholesterol to BAs. *$P < .05$ between groups (n = 7–10 mice/group). PL, phospholipids.

higher in *Cyp2c70*$^{-/-}$ mice compared with WT, whereas triglycerides were lower (Table 1). Hepatic messenger RNA (mRNA) expression levels of genes involved in fatty acid synthesis suggested that de novo lipogenesis (DNL) was decreased in female *Cyp2c70*$^{-/-}$ mice (Figure 7*A*). However, direct quantification of DNL by measuring incorporation of [1-^{13}C]-acetate into fatty acid molecules revealed that the lower hepatic lipid content was primarily due to a reduction of old, preexisting fat (Figure 7*B*).

Mild Portal Fibrosis and Proliferation of Cholangiocytes in Young Adult Cyp2c70$^{-/-}$ Mice

Although young adult *Cyp2c70*$^{-/-}$ mice were not cholestatic, a distinctive hepatic phenotype was evident. The hydrophobic BA pool was associated with mild ductular reactions in 12-week-old mice (Figure 8*A*). Some portal fibrosis and proliferation of cholangiocytes was observed. In agreement with these observations, mRNA expression of *Col1a1*, *Col1a2*, and *Timp1* were increased in *Cyp2c70*$^{-/-}$ mice (Figure 8*B*). Liver weights were higher in female *Cyp2c70*$^{-/-}$ mice, and plasma transaminases were moderately elevated compared with WT littermates in both sexes (Figure 8*C* and *D*), indicating the presence of some liver damage in *Cyp2c70*$^{-/-}$ mice. Intestinal barrier function was clearly impaired in female mice lacking *Cyp2c70*. This effect was less obvious in male *Cyp2c70*-deficient mice due to high variability (Figure 8*E*). Furthermore, spleens were enlarged in *Cyp2c70*$^{-/-}$ mice (Figure 8*F*). Immune cells in a group of female mice were analyzed to investigate whether *Cyp2c70* deficiency was associated with systemic inflammation. Circulating white blood cells were higher in *Cyp2c70*-deficient animals compared with control animals (Figure 9*A*). However, flow cytometry did not reveal altered relative abundances of specific immune cell subsets in blood (Figure 9*B*). In the liver, non–Kupffer cell macrophages were present in increased numbers in mice lacking *Cyp2c70* (Figure 9*C*). Furthermore, CD8$^+$ T cells appeared to be enriched, while CD4$^+$ T cells tended to be reduced in livers of *Cyp2c70*$^{-/-}$ mice. Despite impaired intestinal barrier function in female *Cyp2c70*$^{-/-}$ mice, endotoxin concentrations in portal plasma were below the detection limit (0.15 EU/mL) in these animals.

Cyp2c70 deficiency Is Associated With Marked Changes in Bacterial Colonization of the Gut

Because intestinal microbiota may modulate metabolic and immune functions and BAs can modify microbiome composition,[24] bacterial colonization of the cecum was

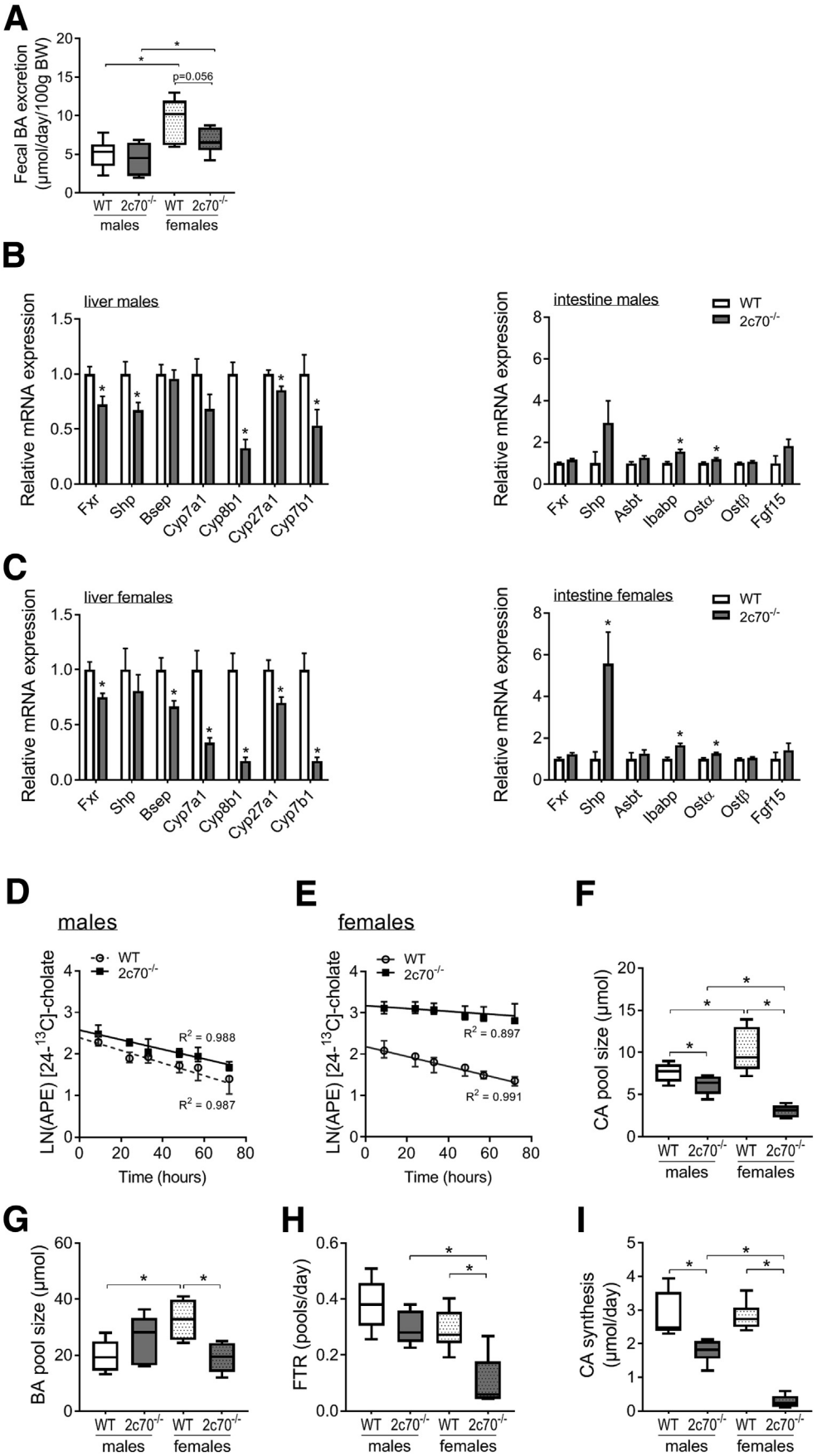

Figure 5. The impact of *Cyp2c70* deficiency on BA metabolism is more pronounced in female mice. Parameters of BA metabolism were assessed in 12-week-old male and female *Cyp2c70*$^{-/-}$ mice and WT littermates. (*A*) Fecal BA excretion. Messenger RNA expression in liver and intestine of (*B*) male and (*C*) female mice. Plasma enrichment of labeled cholic acid following administration of 400 μg [24-^{13}C] cholic acid in (*D*) male and (*E*) female mice. (*F*) Cholic acid pool size. (*G*) Total BA pool size. (*H*) CA turnover rate. (*I*) CA synthesis rate. *$P < .05$ between groups (panels *A–C*, n = 6–10 mice/group; panels *D–I*, n = 5–6 mice/group). APE, atom percent excess; FTR, fractional turnover rate.

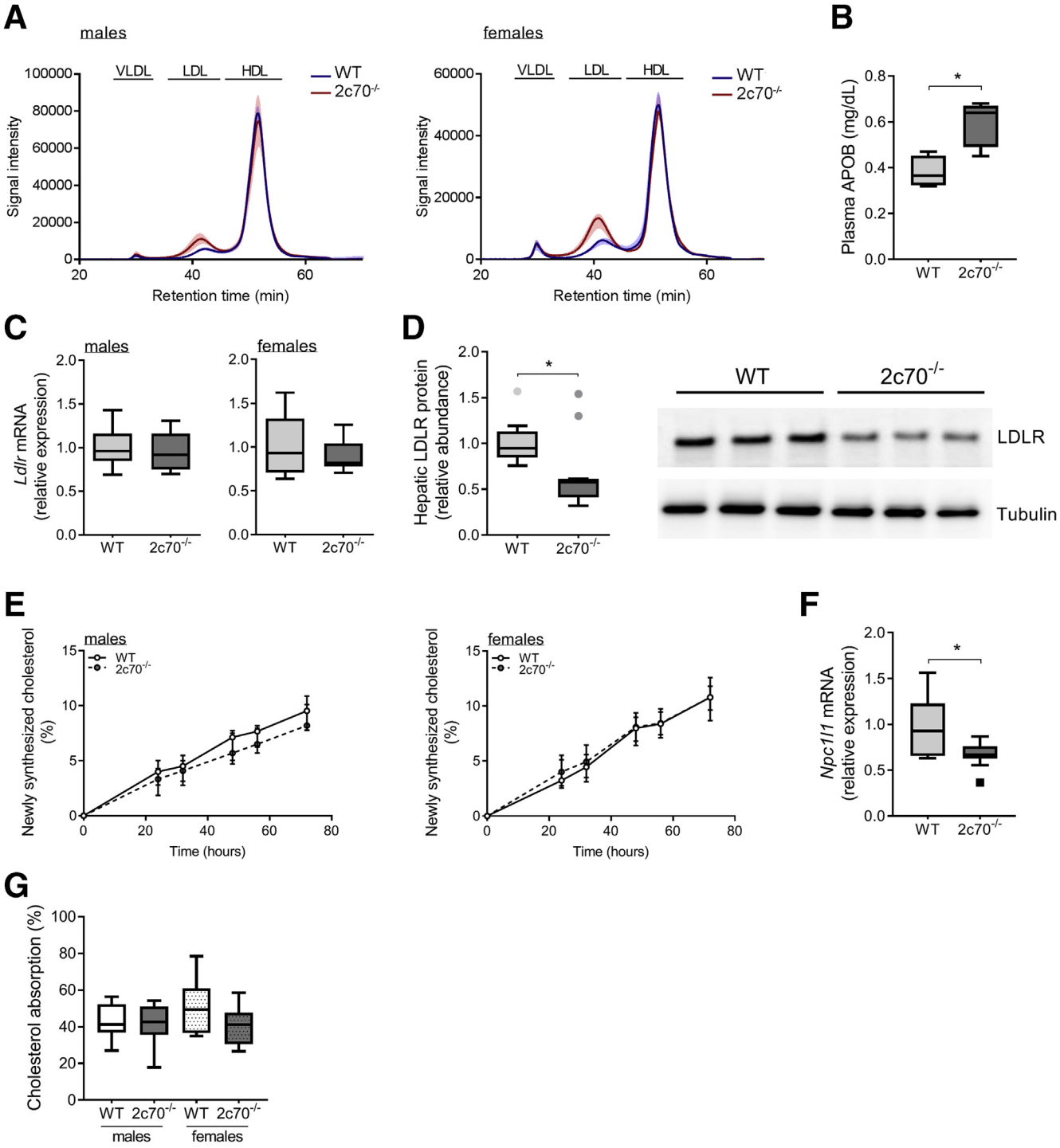

Figure 6. *Cyp2c70*-deficient mice have increased plasma LDL cholesterol levels. Parameters of lipoprotein metabolism were analyzed in 12-week-old *Cyp2c70*$^{-/-}$ mice and WT littermates. (*A*) Cholesterol distribution after lipoprotein fractionation of plasma samples by fast protein liquid chromatography (n = 7–12 mice/group). (*B*) Plasma apolipoprotein B (APOB) protein levels measured using targeted proteomics (n = 4–5 female mice/group). (*C*) Hepatic *Ldlr* mRNA expression levels (n = 7–12 mice/group). (*D*) Hepatic LDLR protein expression in male mice quantified by Western blot (n = 12 mice/group). (*E*) Fractional cholesterol synthesis determined by mass isotopomer distribution analysis following administration of [1-^{13}C]acetate to drinking water of the mice for 3 days (n = 7–11 mice/group). (*F*) *Npc1l1* mRNA expression in the small intestine of female mice (n = 7–10 mice/group). (*G*) Fractional cholesterol absorption determined using orally and intravenously administered stable isotopically labeled cholesterol tracers, as detailed in the Materials and Methods section (n = 7–10 mice/group). *$P < .05$ between groups. HDL, high-density lipoprotein.

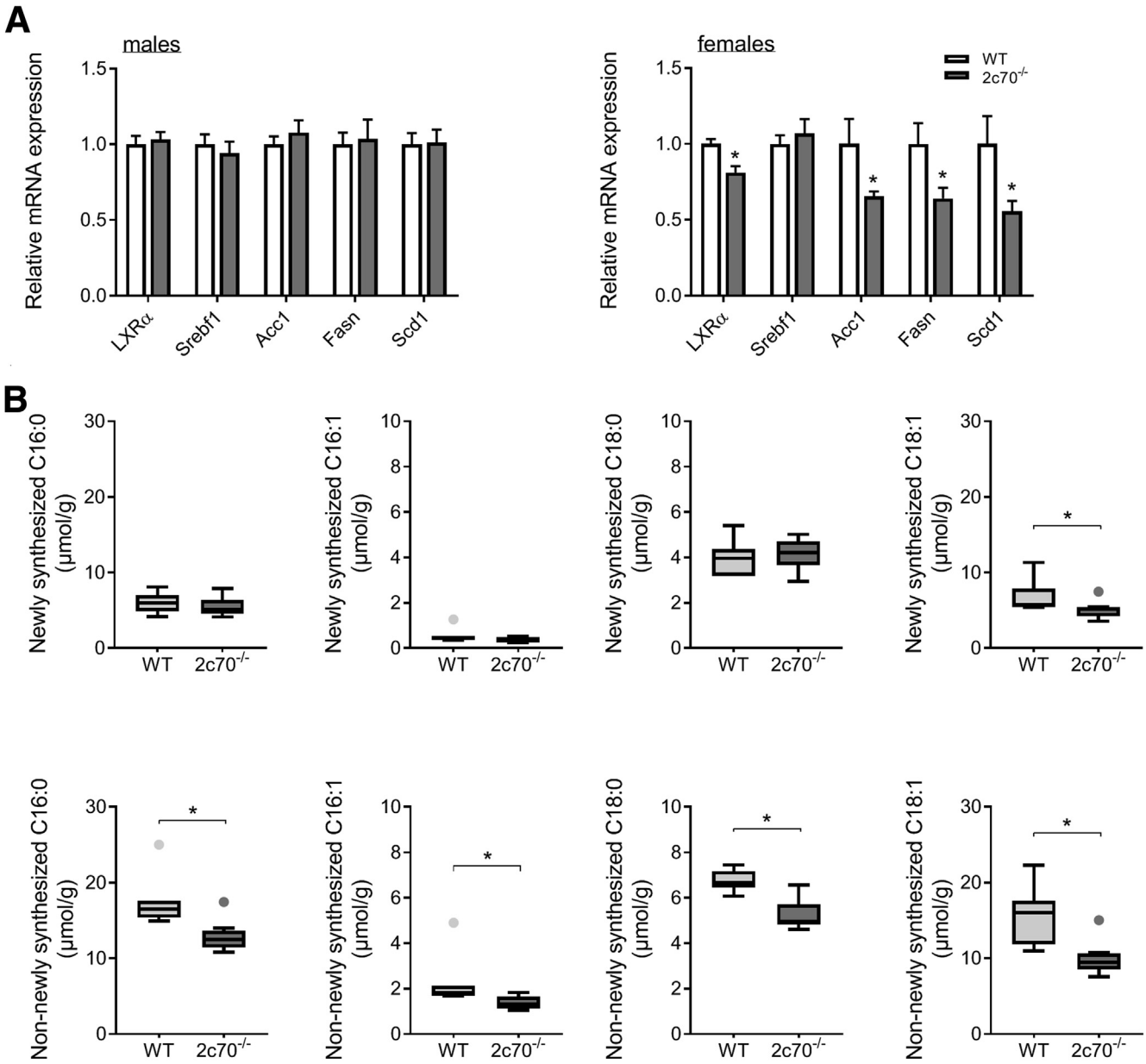

Figure 7. DNL is hardly affected in *Cyp2c70*-deficient mice. (*A*) Hepatic mRNA expression of genes involved in lipid synthesis in 12-week-old *Cyp2c70*$^{-/-}$ mice and WT littermates (n = 7–12 mice/group). (*B*) Hepatic lipid synthesis in 12-week-old female *Cyp2c70*$^{-/-}$ mice and WT littermates quantified following administration of [1-^{13}C]acetate to drinking water (n = 7–10 mice/group). *$P < .05$ between groups.

analyzed in a cohort of male mice. The more hydrophobic BA composition was associated with distinct alterations in the bacterial species present within the gut of *Cyp2c70*$^{-/-}$ mice. Principal coordinates analysis clearly separated *Cyp2c70*$^{-/-}$ from WT mice and hierarchical clustering grouped the mice by genotype (Figure 10*A* and *B*). A total of 46 genera showed differential abundance in *Cyp2c70*$^{-/-}$ mice compared with WT (Figure 11*A*). A number of bacterial species known to produce short-chain fatty acids, including *Roseburia* and *Butyricicoccus*, were more abundant in *Cyp2c70*$^{-/-}$ mice. Other species, including *Akkermansia*, *Rikinella*, and *Christensenellaceae*, were less abundant in the gut of *Cyp2c70*$^{-/-}$ mice, whereas *Prevotella* and *Veillonella* were more prominent in *Cyp2c70*$^{-/-}$ mice compared with control mice (Figure 11*A* and *B*). Several species belonging to the Ruminococcaceae and Lachnospiraceae, reported to exert BA modifying activity,[25] were also more abundant in *Cyp2c70*$^{-/-}$ mice (see Figure 11*A* and *B*).

Marked Preponderance of Liver Disease in Aged Female *Cyp2c70*$^{-/-}$ Mice

Because plasma BA, alanine aminotransferase, and aspartate aminotransferase levels in *Cyp2c70*$^{-/-}$ mice were

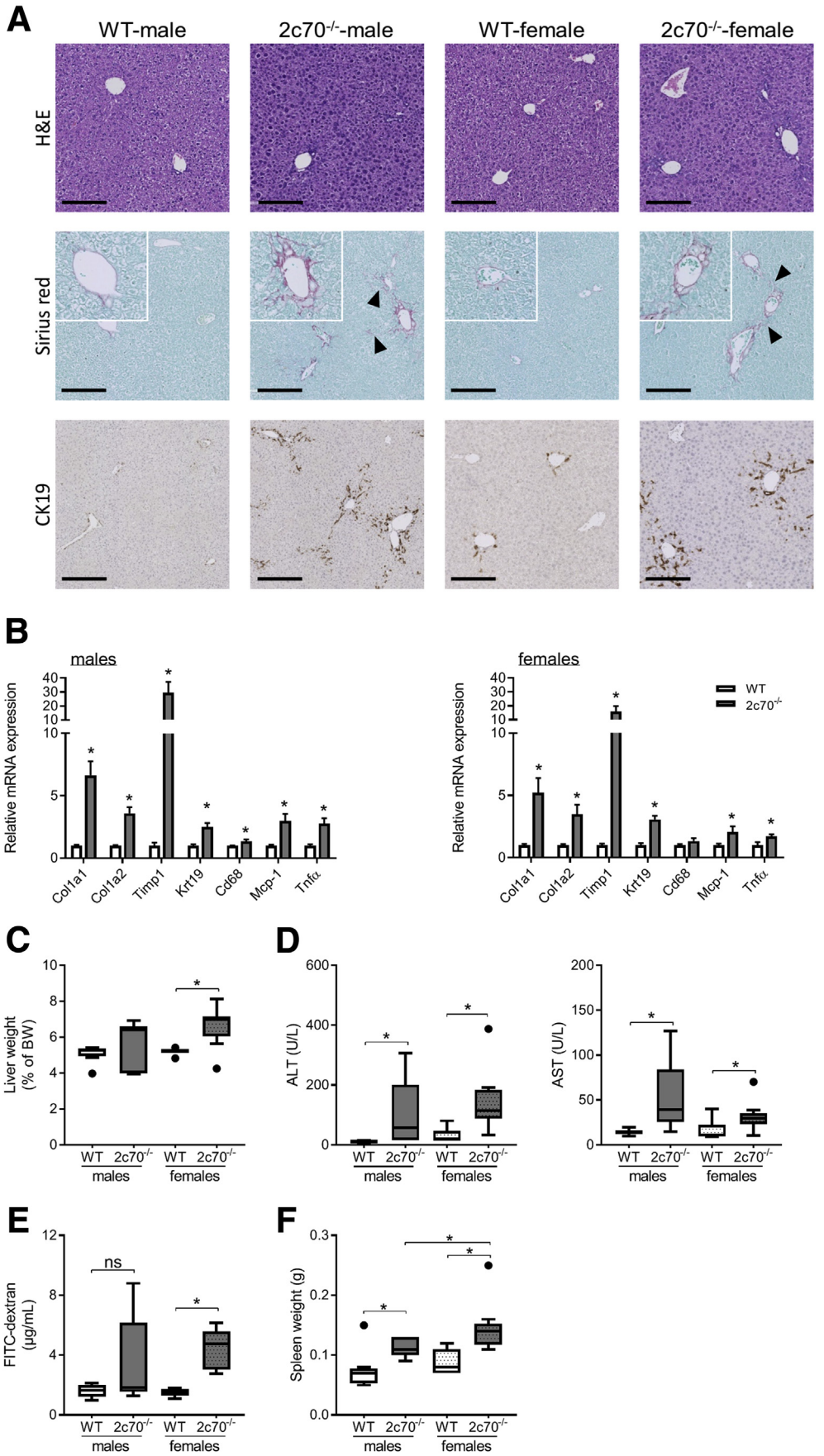

Figure 8. Mild ductular reactions in young adult *Cyp2c70*-deficient mice. Histology and parameters of liver function were assessed in 12-week-old *Cyp2c70*$^{-/-}$ mice and WT littermates. (*A*) Representative images of liver sections from male and female mice stained with hematoxylin and eosin, Sirus red, or an anti-CK19 antibody (black bars represent 200 μm, arrowheads indicate collagen deposition). (*B*) Hepatic mRNA expression of genes involved in fibrosis and inflammation. (*C*) Liver weights. (*D*) Plasma transaminase levels. (*E*) Plasma fluorescence 45 minutes after administration of FITC-Dextran. (*F*) Spleen weights. *$P < .05$ between groups (panels *A–D* and *F*, n = 7–10 mice/group; panel *E*, n = 5–7 mice/group).

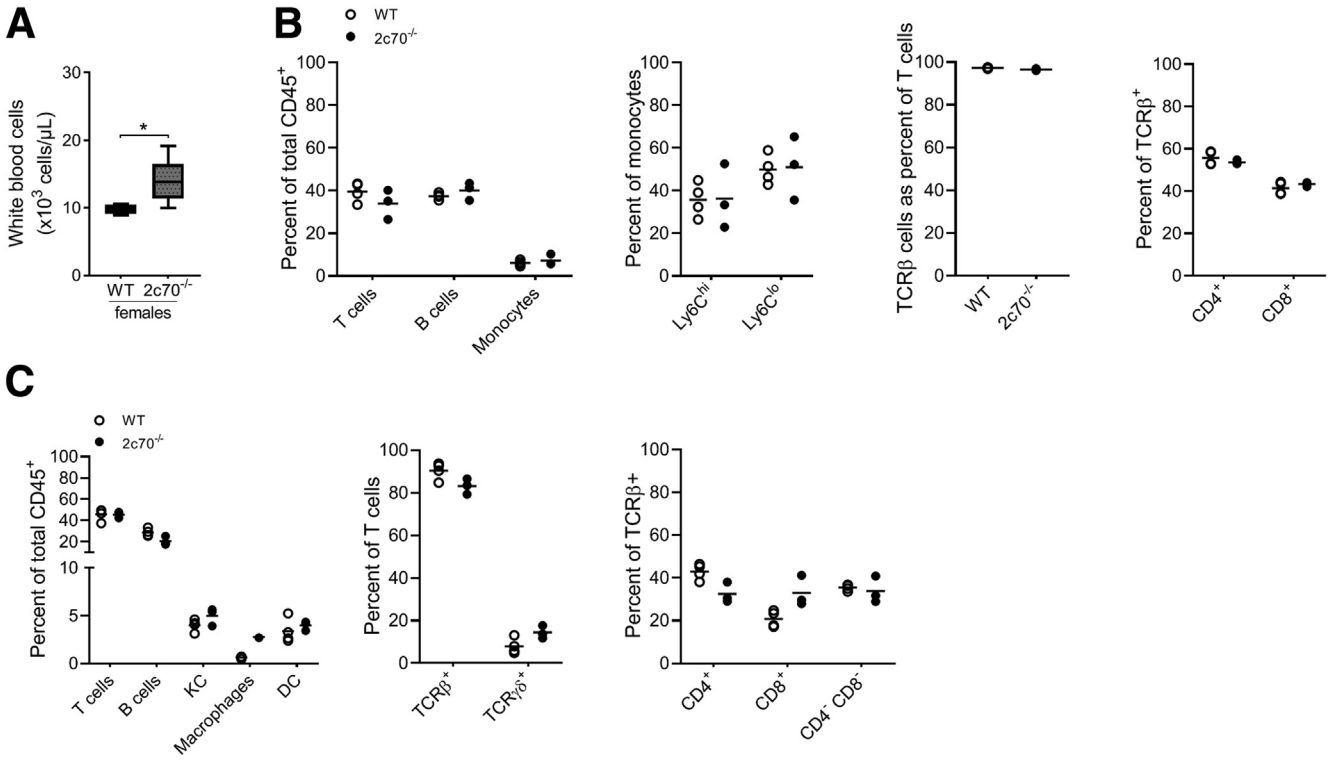

Figure 9. Increased numbers of circulating white blood cells in female *Cyp2c70*-deficient mice. (*A*) White blood cell counts measured in 12-week-old female *Cyp2c70*$^{-/-}$ mice and WT littermates (n = 7–10 mice/group). Immune cell subsets in (*B*) blood and (*C*) liver determined using flow cytometry in female mice of 16 weeks old (n = 3–4 mice/group). *$P < .05$ between groups. DC, dendritic cells; KC, Kupffer cells.

lower at 12 weeks compared with 3 weeks of age, yet still elevated compared with WT animals, we next questioned what would happen to these parameters beyond the young adult state. Therefore, cohorts of mice were aged until 32–34 weeks. Body weights of WT and *Cyp2c70*$^{-/-}$ mice were similar in both genders (Figure 12*A*). However, remarkable differences between sexes became apparent at this advanced age. Male *Cyp2c70*$^{-/-}$ mice showed a normal liver and spleen size and only mildly elevated plasma transaminases, and plasma BA levels comparable to those in WT mice (Figure 12*B–F*). Conversely, female *Cyp2c70*$^{-/-}$ mice had enlarged livers and spleens as well as substantially higher plasma transaminases (Figure 12*B–D*). Plasma BAs in female *Cyp2c70*$^{-/-}$ mice were increased compared with WT control mice and considerably higher than in male *Cyp2c70*$^{-/-}$ mice (Figure 12*E* and *F*). Plasma of male *Cyp2c70*$^{-/-}$ mice contained ~2.5 μmol/L (T)CDCA. However, plasma concentrations of this potent endogenous FXR agonist reached ~100 μmol/L in female *Cyp2c70*$^{-/-}$ mice, while high levels of (T)LCA were present as well. Yet, increased hepatic FXR signaling was not evident, as expression of *Fxr* and its target genes *Shp* and *Bsep* was not increased in either of the genders (Figure 13*A*). Expression of *Cyp8b1* was reduced by ~40% in male *Cyp2c70*$^{-/-}$ mice compared with WT control mice, but was almost completely absent in female mice lacking *Cyp2c70* (Figure 13*A*), indicating very low CA synthesis in these animals. The expression of genes involved in fibrogenesis showed striking differences between male and female *Cyp2c70*$^{-/-}$ mice. In old male *Cyp2c70*$^{-/-}$ mice, *Col1a1*, *Col1a2*, and *Timp1* were only moderately higher than in age- and sex-matched control mice, whereas expression of these genes was increased to a much greater extent in female mice upon *Cyp2c70* deficiency (Figure 13*B*). Expression of the cholangiocyte marker *Krt19*, encoding CK19, showed a similar pattern (Figure 13*B*). In line with the mRNA data, livers of male *Cyp2c70*$^{-/-}$ mice showed near normal liver histology, whereas livers of female *Cyp2c70*-deficient mice displayed bridging fibrosis and had strongly increased numbers of CK19-positive cells (Figure 13*C*). Inflammation markers were mildly increased in both genders in absence of *Cyp2c70* (Figure 13*B*). Together, these results clearly demonstrate that the development of liver disease in *Cyp2c70*$^{-/-}$ mice is sex-dependent, with female mice being substantially more affected than male mice.

Reversal of Liver Disease Associated With Cyp2c70 Deficiency by UDCA

Liver disease and compromised intestinal barrier function in *Cyp2c70*$^{-/-}$ mice may be related to the more hydrophobic composition of the circulating BA pool, but could also result from other, yet unknown, functions of CYP2C70. Therefore, we added 0.1% UDCA to the diet of a cohort of 5-

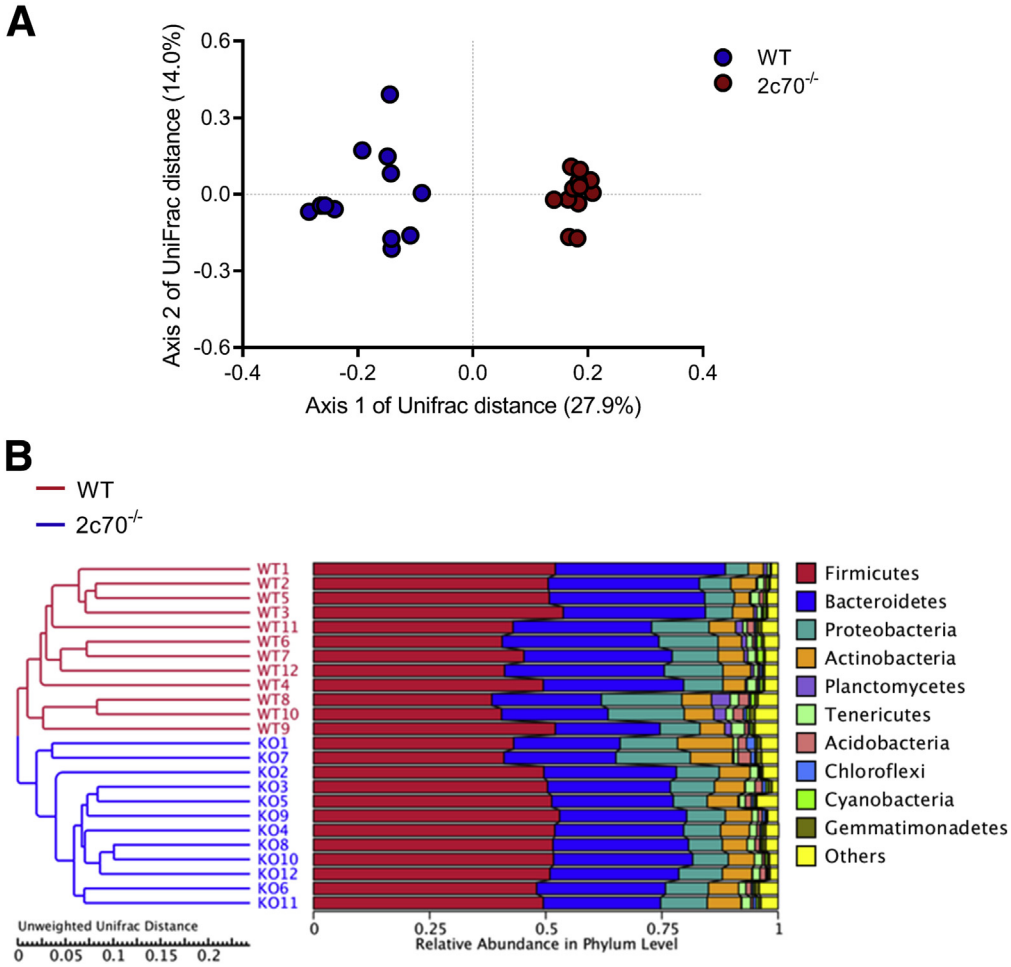

Figure 10. Altered BA composition in *Cyp2c70*-deficient mice impacts bacterial colonization of the gut. Bacterial DNA was isolated from cecal contents of 12-week-old male mice and analyzed by 16S sequencing. (*A*) To compare the overall microbial communities between mice, the unweighted UniFrac distance was calculated based on the taxonomic tree at the genus level using the Phyloseq[49] package for R, and principal coordinates analysis was performed. (*B*) Hierarchical clustering of the mice based on the unweighted UniFrac distance of bacteria present in the cecum of male *Cyp2c70*$^{-/-}$ mice and WT littermates.

week-old female *Cyp2c70*$^{-/-}$ mice until they reached the age of 12 weeks. UDCA accumulated in the BA pool of the treated mice and accounted for ~60% of circulating BAs at the end of treatment in WT and *Cyp2c70*$^{-/-}$ mice (Figure 14*A*). Consequently, the BA pool in the UDCA-treated *Cyp2c70*$^{-/-}$ mice became substantially more hydrophilic (Figure 14*B*). Body weights were not impacted by UDCA treatment (data not shown). Liver sizes of UDCA-treated *Cyp2c70*$^{-/-}$ mice were similar to those of WT animals (Figure 14*C*), and hepatocyte damage was reversed, as evidenced by the complete normalization of plasma transaminases and liver histology (Figure 14*D* and *E*). Ductular reactions and portal fibrosis were no longer observed when *Cyp2c70*$^{-/-}$ mice were treated with UDCA (Figure 14*E*) and expression levels of genes associated with fibrogenesis and inflammation were normalized (Figure 14*F*). In addition, CK19–positive cells in the liver were reduced to normal numbers upon treatment (Figure 14*E*, lower panels), indicating that UDCA corrected cholangiocyte proliferation in *Cyp2c70*$^{-/-}$ mice. To obtain more insight into the changes in the processes underlying the liver pathology in *Cyp2c70*$^{-/-}$ mice and its reversal by UDCA, transcriptome analysis was performed by RNA microarray. Principal component analysis separated the WT mice from the nontreated *Cyp2c70*$^{-/-}$ mice, whereas UDCA-treated *Cyp2c70*$^{-/-}$ mice essentially overlapped with WT mice, indicating that little residual differences in hepatic gene expression were left in UDCA-treated *Cyp2c70*$^{-/-}$ mice (Figure 15*A*). Hierarchical clustering, based on genes that were differentially expressed between groups (false discovery rate [FDR] <5% and a fold-change ≥1.5), clearly separated the nontreated *Cyp2c70*$^{-/-}$ mice from the other groups (Figure 15*B*). Interestingly, UDCA treatment essentially normalized gene expression patterns in *Cyp2c70*$^{-/-}$ mice. Gene set enrichment analysis revealed that pathways involved in extracellular matrix (re)organization were most upregulated in nontreated *Cyp2c70*$^{-/-}$ mice compared with WT control mice, whereas peroxisomal pathways and fatty acid metabolism were among the most downregulated pathways (Figure 16*A*). When *Cyp2c70*$^{-/-}$ mice were treated with UDCA, pathways involved in extracellular matrix (re)organization were no longer among the most altered pathways compared with WT (data not shown) and strongly downregulated compared with untreated *Cyp2c70*$^{-/-}$ mice (Figure 16*B*). UDCA functions as a chaperone and can relieve endoplasmic reticulum (ER) stress.[26] Therefore, we explored whether

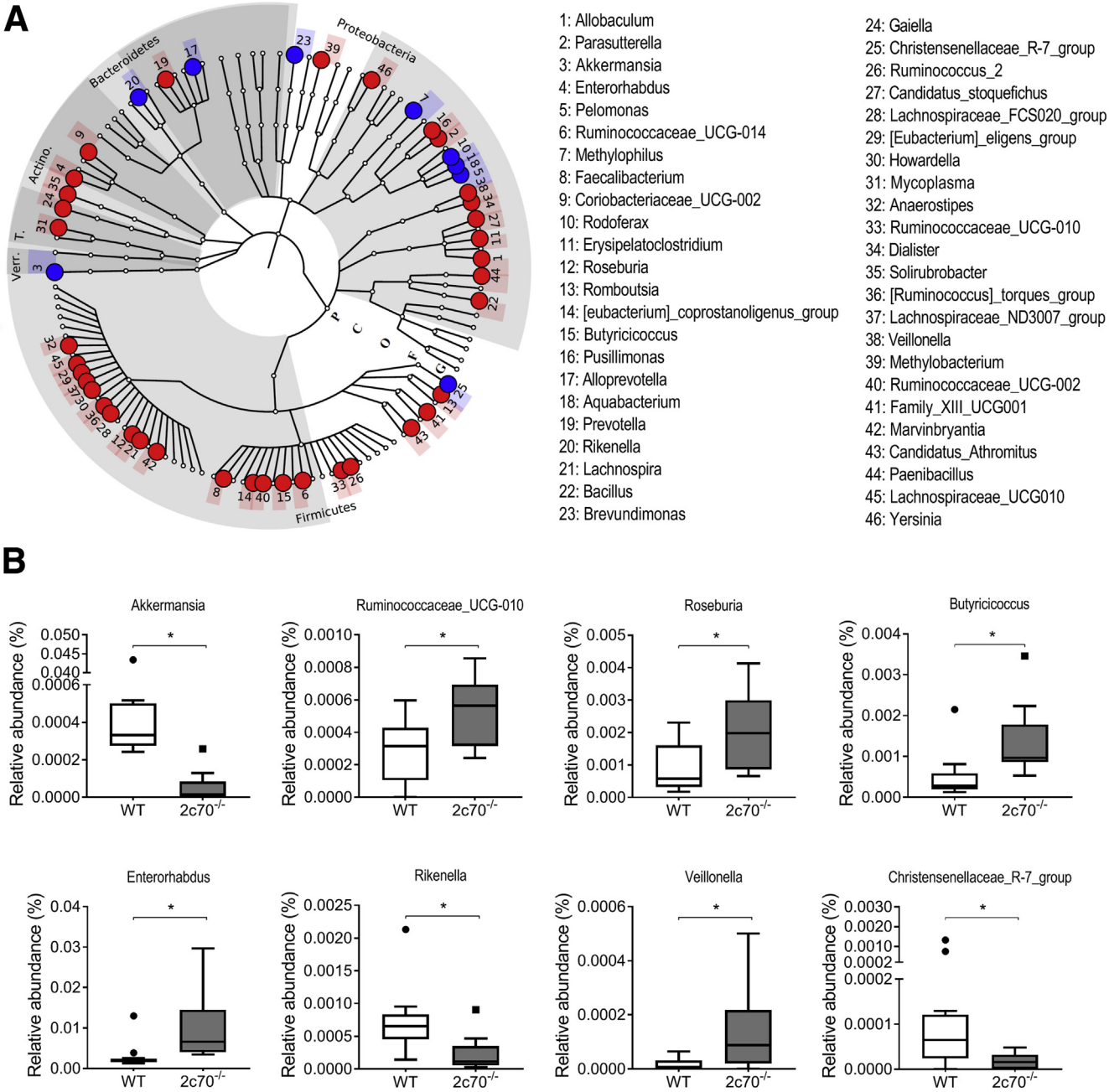

Figure 11. Overview of genera displaying differential abundance in *Cyp2c70*-deficent mice compared with WT littermates. Bacterial DNA was isolated from cecal contents of 12-week-old male mice and analyzed by 16S sequencing. (*A*) Taxonomic cladogram showing the genera that were differently abundant between *Cyp2c70*$^{-/-}$ mice and WT littermates. Genera that were present in increased numbers in *Cyp2c70*$^{-/-}$ mice are shown in red, while genera that were present in lower numbers are depicted in blue. (*B*) Relative abundance of selected genera. *$P_{adj} < .05$ between groups (n = 12 mice/group). Actino., Actinobacteria; C, class; F, family; G, genus; O, order; P, phylum; T., Tenericutes; Verr., Verrucomicrobia.

amelioration of ER stress was involved in the restoration of normal liver physiology in *Cyp2c70*$^{-/-}$ mice by UDCA. Female *Cyp2c70*$^{-/-}$ mice indeed displayed signs of increased ER stress. Hepatic mRNA expression of *Ddit3 (Chop)* showed a tendency toward an increase, and expressions of *Grp78* (*Bip*) and *Dnajc3* (*Hsp40*) were significantly increased in the *Cyp2c70*$^{-/-}$ mice compared with WT animals fed a control diet (Figure 17*A*). Hepatic protein levels of binding immunoglubulin protein (BIP) were also higher in the *Cyp2c70*$^{-/-}$ mice compared control mice (Figure 17*B* and *C*). UDCA treatment rescued the increased expression of these ER stress markers in *Cyp2c70*$^{-/-}$ mice (Figure 17*A*–*C*), suggesting that reduction of ER stress is involved in the reversal of liver pathology in *Cyp2c70*$^{-/-}$ mice. In addition to the normalization of liver physiology by UDCA, spleen size and white blood cell counts returned to normal upon

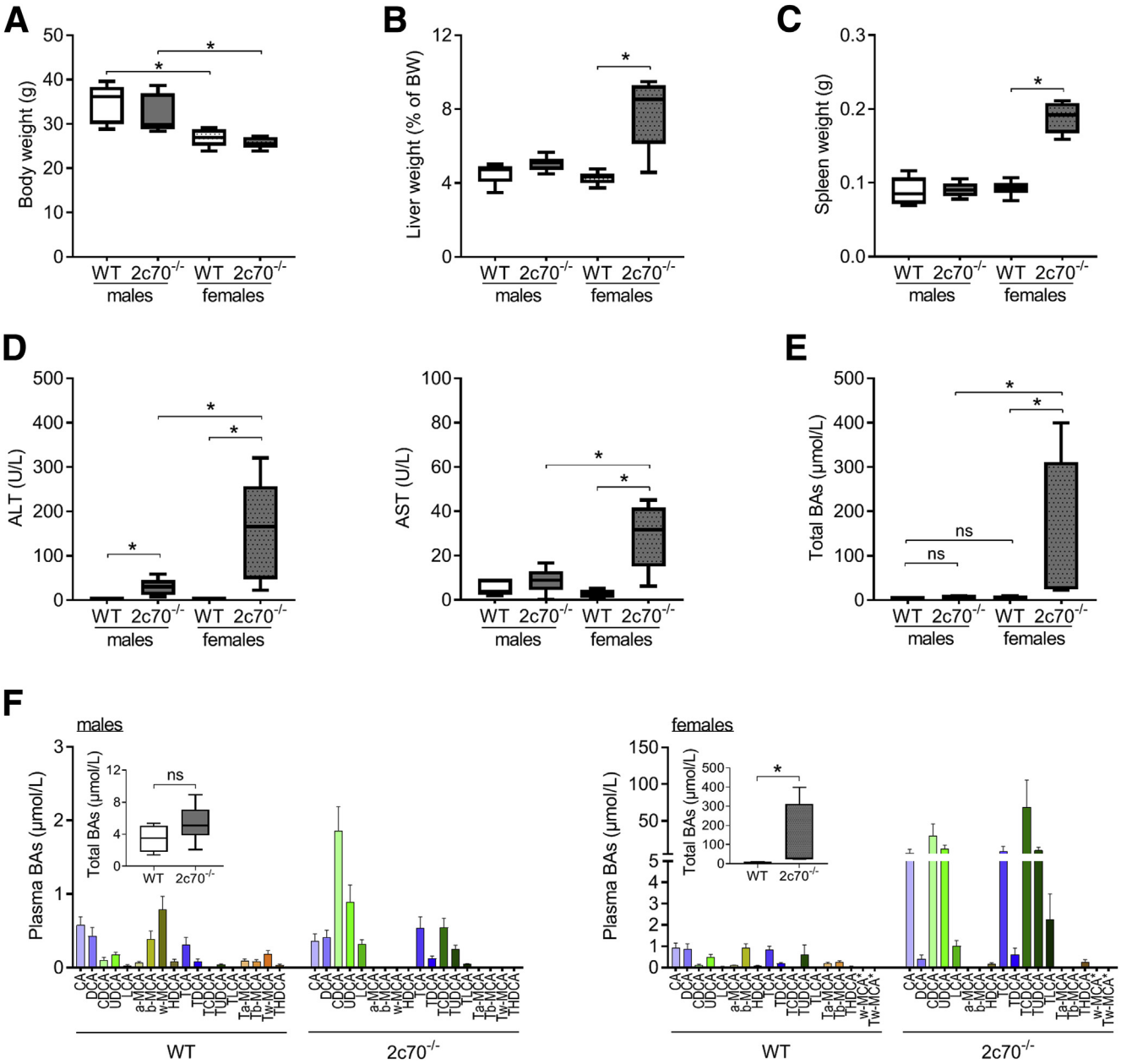

Figure 12. Aged female *Cyp2c70*-deficient mice show marked increases in plasma transaminases and bile. Male and female *Cyp2c70*$^{-/-}$ mice and WT littermates were maintained on a standard rodent diet until they were 32–34 weeks old before they were sacrificed. (*A*) Body weights. (B) Liver weights. (*C*) Spleen weights. (*D*) Plasma transaminase levels. (*E*) Plasma total BA concentrations. (*F*) Plasma BA profiles. *$P < .05$ between groups (n = 4–6 mice/group).

treatment (Figure 18*A* and *B*). The impaired intestinal barrier function observed in *Cyp2c70*$^{-/-}$ mice was corrected by UDCA treatment as well (Figure 18*C*). Taken together, these results indicate that UDCA treatment effectively restores liver and intestinal dysfunction in *Cyp2c70*$^{-/-}$ mice.

Discussion

In the present study, we assessed the (patho)physiological consequences of *Cyp2c70*-deletion in mice in an age- and gender-dependent manner. We show that absence of CYP2C70 leads to a hydrophobic BA pool containing substantial amounts of CDCA and LCA throughout development. *Cyp2c70*$^{-/-}$ mice of both sexes display features of transient "neonatal" cholestasis. Interestingly, the phenotype spontaneously improves into adulthood in male *Cyp2c70*$^{-/-}$ mice, while female *Cyp2c70*$^{-/-}$ mice develop a clear cholangiopathy that progresses to bridging fibrosis at advanced age. The pathologic features in female *Cyp2c70*$^{-/-}$ mice could, however, be fully reversed by treatment with UDCA.

The differences in BA composition between humans and mice result in marked disparity in physicochemical

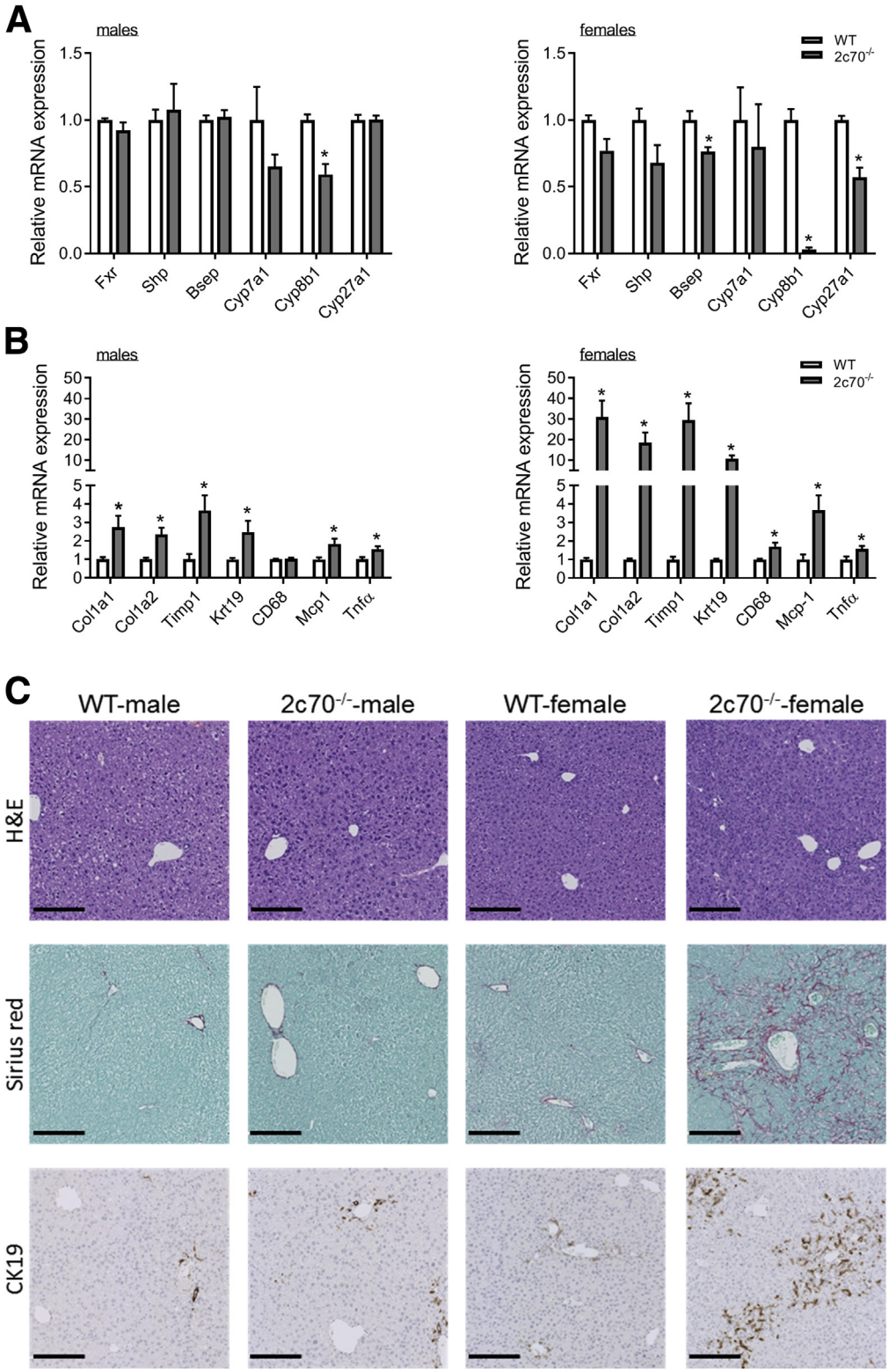

Figure 13. Female but not male *Cyp2c70*-deficient mice display marked liver pathology at advanced age. Hepatic mRNA expression levels of genes involved in (*A*) BA metabolism and (*B*) fibrogenesis and inflammation in 32- to 34-week-old *Cyp2c70*$^{-/-}$ mice and WT littermates. (*C*) Representative images of liver sections from these aged mice stained with hematoxylin and eosin, Sirus red, or an anti-CK19 antibody (black bars represent 200 μm). *$P < .05$ between groups (n = 4–6 mice/group).

characteristics of the circulating BA pools.[3] This obviously complicates translation of preclinical observations, eg, data concerning effects of pharmacological FXR modulation[3], to the human situation. "Humanization" of BA metabolism in mice by knocking out *Cyp2c70* can facilitate translation of murine data while preserving the benefits of the mouse as a preclinical model, such as the possibilities for selective genetic modifications. Hence, *Cyp2c70*$^{-/-}$ mice represent an

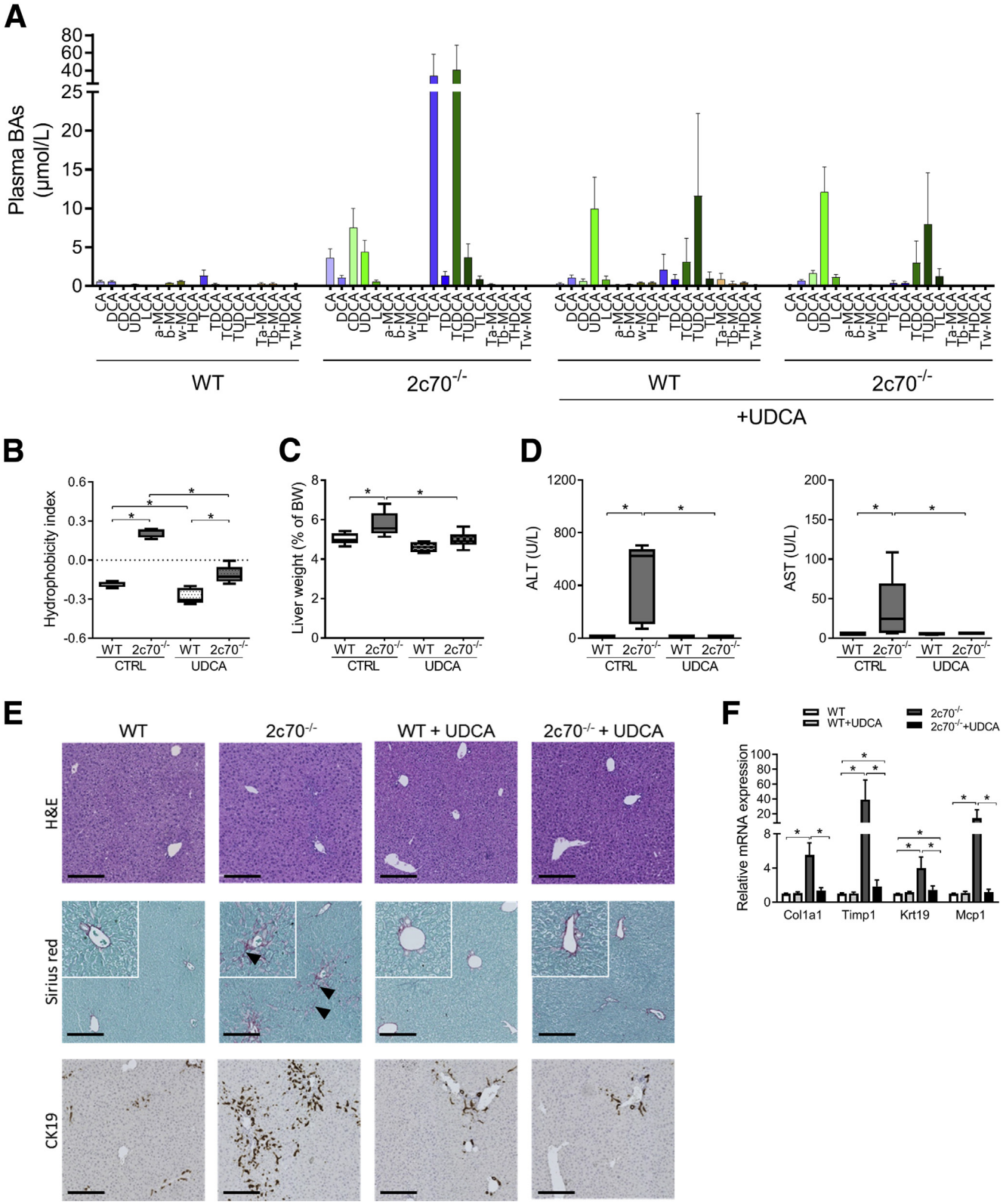

Figure 14. UDCA reverses cholangiopathy in female *Cyp2c70*-deficient mice. Female *Cyp2c70*$^{-/-}$ mice and WT littermates were fed a diet with 0.1% UDCA or a control diet from 5 to 12 weeks of age. BA composition was measured and parameters related to liver function were assessed at the age of 12 weeks. (*A*) BA profiles in plasma. (*B*) Hydrophobicity index of biliary BAs. (*C*) Liver weights. (*D*) Plasma transaminases. (*E*) Representative images of liver sections stained with hematoxylin and eosin, Sirus red, or an anti-CK19 antibody (black bars represent 200 μm, arrow heads indicate collagen deposition). (*F*) Hepatic mRNA expression levels of genes involved in fibrogenesis and inflammation. *$P < .05$ between groups (n = 5–6 mice/group). CTRL, control.

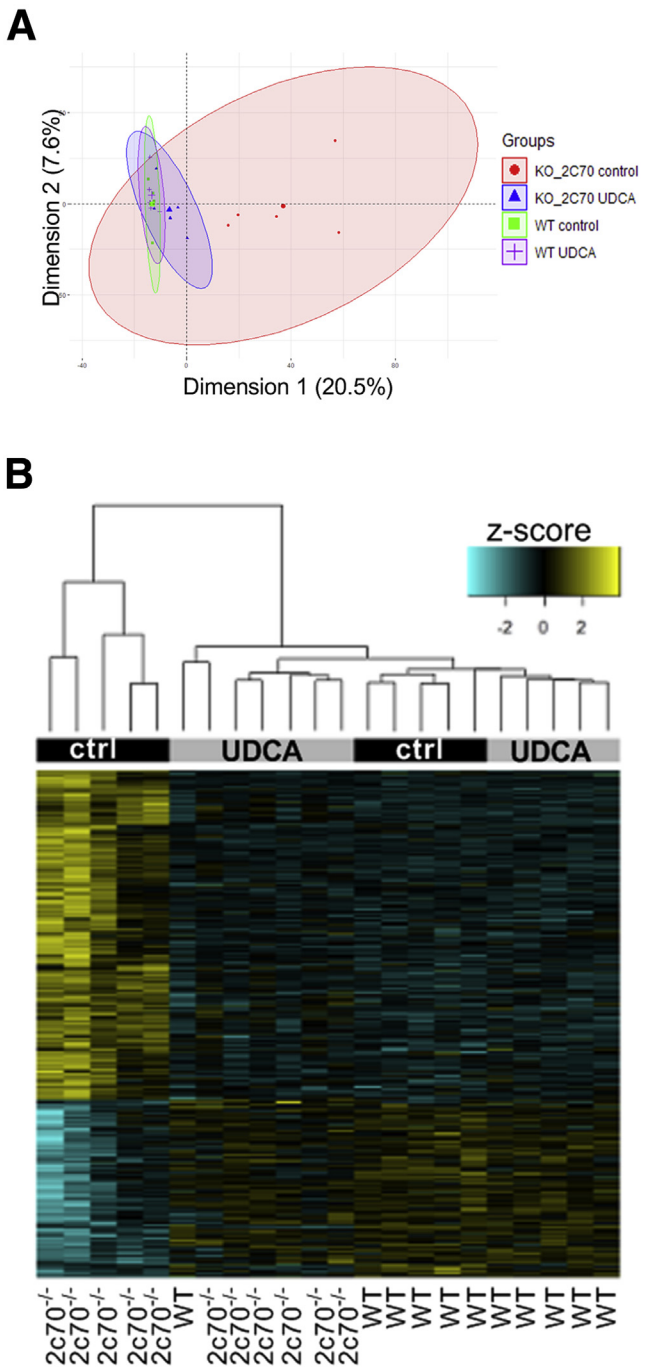

Figure 15. UDCA normalizes hepatic gene expression patterns in female *Cyp2c70*-deficient mice. (*A*) Principal component analysis of hepatic mRNA microarray data obtained from 12-week-old female *Cyp2c70*$^{-/-}$ mice and WT littermates treated with and without 0.1% UDCA in their diet from 5 to 12 weeks of age. (*B*) Hierarchical clustering of mice based on genes that were differentially expressed between groups using an FDR cutoff of 5% and a fold-change >1.5 (n = 5–6 mice/group).

interesting model to study BA-related liver diseases and could also be employed to explore the impact of BAs and pharmacological manipulations of BA signaling pathways on metabolism. Not surprisingly, therefore, several research groups[5–7] have recently generated mice that specifically lack *Cyp2c70*.

The BA pool of *Cyp2c70*$^{-/-}$ mice contained considerable amounts of hydrophobic CDCA and LCA and therefore had a much higher cytotoxic potential than the BA pool in WT mice.[27] Oval cell proliferation has indeed been reported in livers of *Cyp2c* cluster *null* mice[28] and *Cyp2c70*$^{-/-}$ mice,[6] but the (patho)physiological consequences of the more hydrophobic BA pool in *Cyp2c70*$^{-/-}$ mice have remained ill defined. In the current study, we demonstrate that *Cyp2c70*$^{-/-}$ mice of both sexes display transient "neonatal" cholestasis. Intriguingly, marked differences between genders became apparent when age-dependent consequences of *Cyp2c70* deficiency were assessed. Female, but not male, *Cyp2c70*$^{-/-}$ mice displayed progression of liver disease and bridging fibrosis at more advanced ages. Furthermore, female *Cyp2c70*$^{-/-}$ mice had a markedly reduced total BA pool size compared with WT control mice, whereas the pool size was not impacted by *Cyp2c70*-deletion in male mice. Hence, the overall impact of *Cyp2c70*-deletion was more pronounced in female mice compared with male mice in our studies. Honda et al[6] recently reported ductular reactions in male *Cyp2c70*$^{-/-}$ mice, whereas female mice showed a more variable phenotype. In contrast to our study, these authors only studied mice at young adult age and did not assess fibrosis development. The reason for the more pronounced phenotype in adult female *Cyp2c70*$^{-/-}$ mice in our studies remains elusive, but the minimal phenotypic differences between male and female *Cyp2c70*$^{-/-}$ mice at 3 weeks of age suggest involvement of sex hormones in the development of liver pathology in female *Cyp2c70*$^{-/-}$ mice at more advanced ages. Interestingly, estrogen was shown to repress the expression of *Cyp8b1* in bile-diverted rats.[29] Indeed, the ratio of 12α-hydroxylated to non-12α-hydroxylated BAs was lower in *Cyp2c70*-deficient female mice compared with male mice. However, the differences in 12α-hydroxylation between male mice and female mice only appeared upon *Cyp2c70*-ablation (Figure 1*B*) despite similar hepatic expression levels of *Cyp2c70* in both sexes in C57BL/6 mice.[30]

The BA pool in *Cyp2c70*$^{-/-}$ mice clearly comprises more potent FXR agonists than the pool of WT mice. Yet, in line with our previous findings[5] as well as with data reported by others,[6,7] this did not translate into evidently increased hepatic FXR activation. In the ileum, we did observe increased expression of multiple FXR target genes in *Cyp2c70*$^{-/-}$ mice, but expression of *Fgf15*, important in control of hepatic BA synthesis, was hardly affected. Nevertheless, mRNA expression levels of key enzymes in the BA synthesis pathways were clearly reduced in *Cyp2c70*$^{-/-}$ mice. Taken together, the impact of the more human-like BA composition on the regulation of BA synthesis appears to be complex and requires more investigation.

In apparent contrast to the dogma that hydrophobic BAs facilitate intestinal lipid absorption more efficiently than hydrophilic ones,[31] we did not observe increased fractional cholesterol absorption in *Cyp2c70*$^{-/-}$ mice compared with WT control mice. Decreased expression of the cholesterol uptake transporter *Npc1l1* in the proximal small intestine

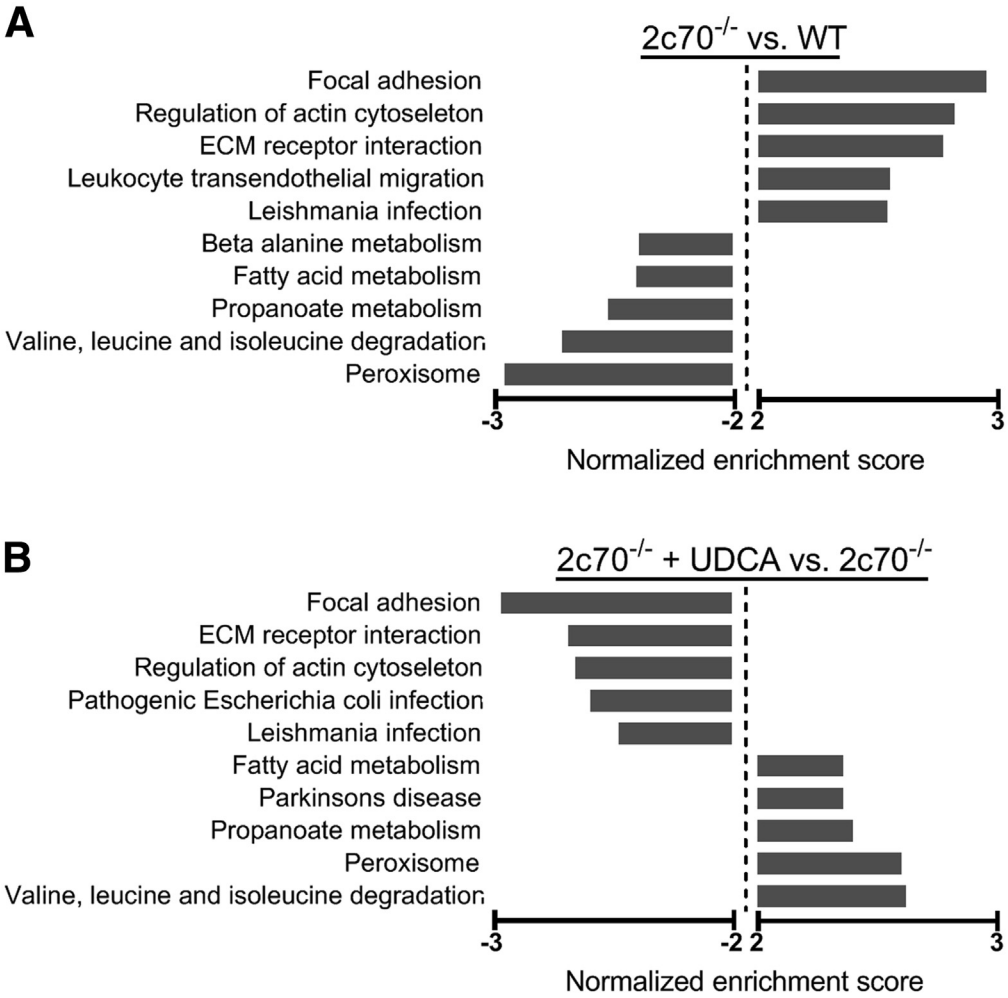

Figure 16. UDCA treatment corrects the increase in expression of gene sets involved in extracellular matrix (re) organization in female *Cyp2c70*-deficient mice. Gene set enrichment analysis based on hepatic mRNA microarray data obtained from female *Cyp2c70*$^{-/-}$ mice and WT control mice with and without addition of 0.1% UDCA to the food from 5 to 12 weeks of age (n = 5–6 mice/group). ECM, extracellular matrix.

may have counteracted the effects of the hydrophobic BA pool in *Cyp2c70*$^{-/-}$ mice. Others[6,7] recently reported reduced levels of plant sterols, which are used as surrogate markers of cholesterol absorption, in plasma of *Cyp2c70*$^{-/-}$ mice compared with control mice, suggesting decreased cholesterol absorption. This was, however, not apparent from our direct measurements of fractional cholesterol absorption.

BAs are known to impact the gut microbiome.[32] Because the bactericidal properties differ between BA species,[32] we

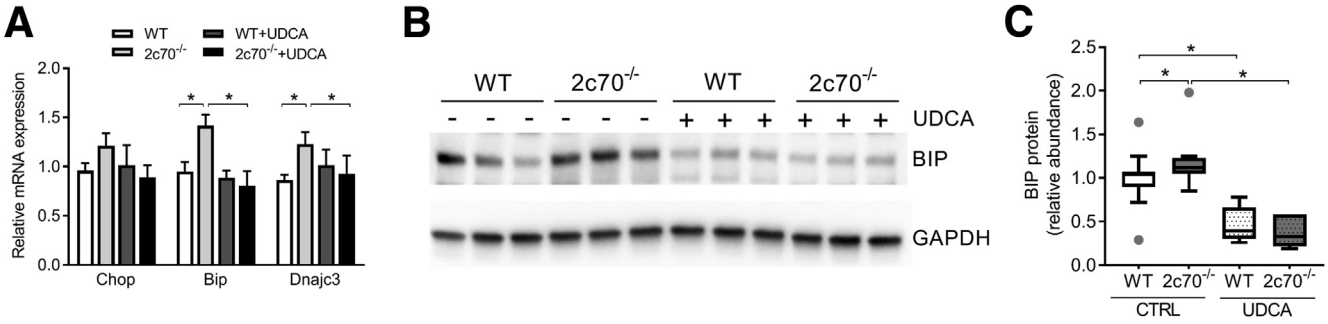

Figure 17. Elevation of ER stress markers in female *Cyp2c70*-deficient mice is corrected by UDCA. Livers of 12-week-old female *Cyp2c70*$^{-/-}$ mice and WT littermates fed a diet with 0.1% UDCA or a control diet from 5 to 12 weeks of age were harvested and markers of ER stress were analyzed. (*A*) Hepatic mRNA expression of ER stress markers. (*B*) Representative Western blot for BIP on liver material. (*C*) Relative hepatic BIP protein levels quantified based on the Western blot data in panel *B* using GAPDH to correct for loading differences. *$P < .05$ between groups (n = 5–12 mice/group).

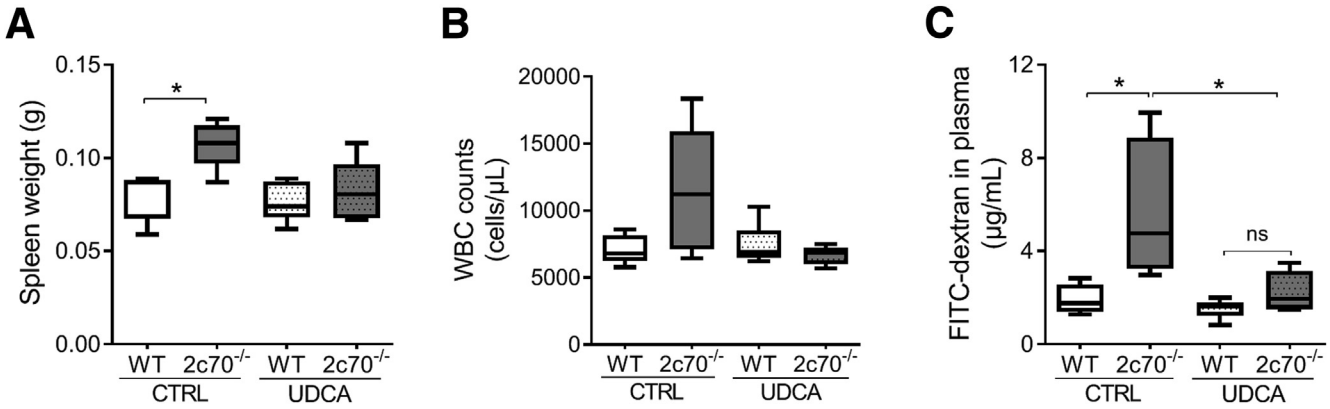

Figure 18. UDCA restores intestinal barrier function in female *Cyp2c70*-deficient mice. (*A*) Spleen weights and (*B*) white blood cell counts in 12-week-old female *Cyp2c70*$^{-/-}$ mice and WT littermates fed a diet with or without 0.1% UDCA from 5 to 12 weeks of age. (*C*) Plasma fluorescence 45 minutes after administration of FITC-Dextran to these mice, measured at the age of 11 weeks. *$P < .05$ between groups (n = 5–6 mice/group). WBC, white blood cell.

hypothesized that the altered composition of the BA pool in *Cyp2c70*$^{-/-}$ would affect the microbial community in the gut. Indeed, differences in bacterial colonization of the intestinal tract were observed between *Cyp2c70*$^{-/-}$ mice and their WT littermates. Genera of *Akkermansia*, *Rikinella*, and *Christensenellaceae* were less abundant, while *Prevotella* and *Veillonella* were more abundant in *Cyp2c70*$^{-/-}$ mice compared with control mice. Interestingly, the abundances of these genera were recently reported to be changed in similar directions in the gut of PBC patients compared with healthy control mice.[33] The bacterial signature in *Cyp2c70*$^{-/-}$ mice thus appears to show certain similarities with the alterations in gut colonization observed in PBC patients.[33] *Akkermansia muciniphila* contributes to maintenance of barrier integrity in the gut.[34] Although 16S DNA sequencing does not allow quantification of individual bacterial species, it is tempting to speculate that the strong reduction of the abundance of species belonging to the genera *Akkermansia* may have contributed to the increased intestinal permeability observed in *Cyp2c70*$^{-/-}$ mice.

Although the physicochemical properties of the BA pool in *Cyp2c70*$^{-/-}$ mice are considerably more similar to humans than those of the pool in WT mice, certain differences in BA metabolism between *Cyp2c70*$^{-/-}$ mice and humans do remain. *Cyp2c70*$^{-/-}$ mice are able to rehydroxylate DCA and therefore still have a slightly more hydrophilic BA pool than humans. While this manuscript was in preparation, CYP2A12 was identified as the enzyme responsible for the conversion of DCA into CA in mouse livers by 7α-rehydroxylation.[6] Another difference between *Cyp2c70*$^{-/-}$ mice and humans concerns the conjugation of BAs in the liver. Although BAs are predominantly conjugated to taurine in human neonates,[35] glycine conjugation predominates in humans >1 year old. Glycine-conjugated BAs are only slightly more hydrophobic than their taurine-conjugated counterparts.[10] Despite these differences, the hydrophobicity index of biliary BAs in *Cyp2c70*$^{-/-}$ mice (~+0.2) is more comparable to that of humans (~+0.3)[10] than to that of WT mice (~−0.3). The physicochemical characteristics of the BA pool in *Cyp2c70*$^{-/-}$ mice thus closely resemble those of the human BA pool. *Cyp2c70*$^{-/-}$ mice therefore represent a valuable model to study BA-related liver diseases and metabolic actions of BAs in vivo. The cholangiopathy that is observed in female mice upon "humanization" of the BA pool obviously represents a point of concern for their application in metabolism-oriented preclinical studies.[19] Interestingly, these phenotypic distortions could be fully restored by adding 0.1% UDCA to the diet. Thus, our data indicate that altered composition of the BA pool indeed caused the cholangiopathy rather than other, yet unknown, functions of CYP2C70. Consequently, it would be interesting to investigate to what extend variations in BA composition between human subjects affect their risk of developing liver disease (eg, whether people with a high relative abundance of hydrophobic CDCA are at increased risk). The mechanism by which UDCA restores liver physiology in *Cyp2c70*$^{-/-}$ mice might involve reduction of ER stress, as UDCA is known to ameliorate ER stress by acting as a chemical chaperone.[26] Indeed, UDCA treatment alleviated the signs of ER stress in the livers of female *Cyp2c70*$^{-/-}$ mice. It is likely that elevated LDL cholesterol levels in *Cyp2c70*$^{-/-}$ mice are related to an ER stress-induced decrease of LDLR protein levels (eg, due to increased occupancy of the chaperone GRP94 by misfolded proteins), resulting in a reduction of its inhibitory interaction with intracellular PCSK9 and, hence, in reduced protection of LDLR from PCSK9-induced degradation.[36] In line with this hypothesis, LDL cholesterol was reduced to normal levels upon UDCA treatment. UDCA was provided from 5 to 12 weeks of age in our experiments. It would be interesting to study whether UDCA would also be able to fully prevent the aging-associated liver pathology in female *Cyp2c70*$^{-/-}$ mice by extending treatment beyond 12 weeks of age.

Taken together, chow-fed *Cyp2c70*$^{-/-}$ mice develop liver pathology in a sex-specific manner. Multiple characteristics of the development of the hepatic phenotype in *Cyp2c70*$^{-/-}$ mice are similar to those in humans with PBC, including female preponderance of liver disease and beneficial effects

of UDCA on liver function. *Cyp2c70*$^{-/-}$ mice may thus serve as a model for PBC and be used to study other BA-related liver pathologies such as progressive familiar intrahepatic cholestasis. For instance, crossbreeding of *Cyp2c70*$^{-/-}$ mice with mice lacking the bile salt export pump (BSEP) could be envisioned to serve as a preclinical model for progressive familiar intrahepatic cholestasis. Besides, modulation of CYP8B1 activity in *Cyp2c70*$^{-/-}$ mice could be employed to assess the impact of BA pool composition on insulin resistance and energy homeostasis. Furthermore, *Cyp2c70*$^{-/-}$ mice are anticipated to be very instrumental for the study of the versatile interactions between BAs, the gut microbiome and host metabolism. Such future studies may contribute to delineation of the underlying reasons for the observed marked differences between male and female *Cyp2c70*$^{-/-}$ mice. Elucidation of these mechanisms fell beyond the scope of the current study, but clarification of the interactions between sex hormones and BA metabolism as well as of potential sex differences in the interactions between BAs and the intestinal microbiome in these mice will be subject of our future studies.

Materials and Methods

Animals

Cyp2c70 knockout mice were generated using CRISPR/Cas9-technology. Zygotes were isolated from a female C57BL/6J mouse 1 day after fertilization and injected with a mRNA encoding the Cas9 endonuclease as well as a sgRNA (5′-CCCACTCCTTTACCAATTGT-3′) directed against the *Cyp2c70* gene. The zygotes were then transplanted into the infundibulum of a pseudo pregnant B6CBAF1/J mouse. The targeted region of the *Cyp2c70* gene was sequenced in the offspring and mosaic mice were crossed with WT C57BL/6J mice to obtain heterozygous founders.

Animals were housed under climate-controlled conditions (21°C) with a 12-hour light/dark day/night-cycle. Animals had ad libitum access to a standard rodent diet (RM-1; Special Diet Services, Essex, United Kingdom) during the experiments. When indicated, 0.1% UDCA (w/w) (Sigma-Aldrich, St Louis, MO) was mixed into the food. Bile cannulations were performed in dedicated cohorts of 12-week-old mice. These mice were anesthetized by intraperitoneal injection of Hypnorm (fentanyl/fluanisone; 1 ml/kg) and diazepam (10 mg/kg) prior to ligation of the common bile duct and cannulation of the gallbladder. Directly after cannulation, mice were placed in a humidified incubator to maintain body temperature. Bile that was secreted during the first 5 minutes was discarded to prevent collection of, more concentrated, gallbladder bile. Next, hepatic bile was collected continuously for 30 minutes. Bile production was determined gravimetrically, whereas concentrations of BAs, phospholipids and cholesterol in the bile were determined as described subsequently. Animal experiments were performed in accordance with the Dutch law and were approved by the Dutch Central Committee for Animal Experiments and the Animal Welfare Body of the University of Groningen.

Targeted Proteomics

Protein levels of CYP2C70 and APOB were quantified by targeted proteomics[37] using an isotopically labeled peptide (TDSSLLSR; Thermo Fisher Scientific, Rockford, IL) for CYP2C70 and a labeled concatemer-derived peptide (QSFDLSVK; PolyQuant GmbH, Bad Abbach, Germany) for apolipoprotein B as standards.

Western Blot

Total protein was isolated from liver homogenates (10%, w/w) and quantified using the Pierce BCA protein assay kit (Thermo Fisher Scientific, Waltham, MA). Equal amounts of protein (~20 μg) were separated by size using sodium dodecyl sulfate polyacrylamide gel electrophoresis and transferred onto nitrocellulose membranes. Membranes were blocked with 5% skim milk in Tris-buffered saline containing 0.1% Tween-20 for 1 hour and subsequently incubated with anti-LDLR (PAB8804, 1:1000; Abnova, Taipei, Taiwan), anti-BIP (3177S, 1:1000; Cell Signaling Technology, Danvers, MA), anti-tubulin (2144S, 1:1000; Cell Signaling Technology) or anti-GAPDH (1:2000, CB1001; Millipore, Burlington, MA) overnight at 4°C. Horseradish peroxidase–conjugated secondary antibodies were then added to detect the proteins of interest. Antibody binding was visualized using SuperSignal West Femto substrate (Thermo Fisher Scientific, Waltham, MA), and signal quantitation was carried out using the freely available ImageJ software (v1.53a, National Institutes of Health, Bethesda, MD).

Plasma Parameters

Plasma triglycerides, free fatty acids, total cholesterol, and free cholesterol were measured using commercially available kits (DiaSys Diagnostic Systems, Holzheim, Germany; Roche Diagnostics, Basel, Switzerland). Plasma lipoproteins were separated by fast protein liquid chromatography using a system containing a PU-4180 pump with a linear degasser and UV-4075 UV/VIS detectors (Jasco, Tokyo, Japan), as described.[38] Plasma (25 μL) was diluted with phosphate-buffered saline (PBS) (pH 7.4) in a 1:1 ratio before being loaded onto the column (Superose 6 Increase 10/300 GL; GE Healthcare, Hoevelaken, the Netherlands). Lipoproteins were then separated using PBS (pH 7.4, flow rate of 0.31 mL/min) as eluent. Total cholesterol concentrations were quantified using a colorimetric reagent (11489232; Roche Diagnostics) that was added in line at a rate of 0.1 mL/min using an additional PU-4080i infusion pump (Jasco). Data acquisition and analysis were performed using ChromNav software (version 1.0; Jasco).

Plasma transaminases were analyzed using a Cobas 6000 analyzer with standard reagents (Roche Diagnostics). Endotoxin was measured using Endosafe limulus amebocyte lysate cartridges for the Nexgen-PTS (Charles River, Leiden, the Netherlands) after a dilution of 30× in limulus amebocyte lysate water.

Measurement of BAs, Neutral Sterols, and Biliary Phospholipids

BAs in plasma and bile were measured by ultra high-performance liquid chromatography tandem mass

spectrometry,[5] while fecal BAs were quantified by gas-liquid chromatography.[5] Biliary cholesterol concentrations were determined by gas-liquid chromatography as described elsewhere.[37] Biliary phospholipids were determined as described.[39]

Real-Time Quantitative Polymerase Chain Reaction

Real-time quantitative polymerase chain reaction was performed on reverse transcribed RNA using either TaqMan primer-probe combinations (Applied Biosystems, Foster City, CA) or SYBR green mastermix (Roche Diagnostics). Data were normalized to cyclophilin as a housekeeping gene.

Microarray Analysis

Transcriptome analysis of livers obtained from female *Cyp2c70*$^{-/-}$ mice and WT littermates, fed a diet with or without 0.1% UDCA from 5 to 12 weeks of age, was performed using Mouse Gene 2.0ST arrays (Affymetrix; Thermo Fisher Scientific) as described.[40] The MADMAX[41] pipeline was used for processing microarray data. After normalization, differentially expressed genes were extracted using IBMT statistics[42] with the FDR cutoff set at 5%. Gene set enrichment analyses[43] were performed using the C2 canonical KEGG pathways. A heat map of differentially expressed genes was generated following processing of array data with Bioconductor[44] and normalization of gene expression using robust multichip averaging.[45] Differential gene expression between groups was assessed using limma[46] with the FDR set at 5% (and a fold-change cutoff of 1.5). Hierarchical clustering of differentially expressed genes was carried out using the *hopach* package[47] with the cosine distance metric. The raw data were deposited in the GEO database (GSE138779).

Histology

Formalin-fixed, paraffin-embedded sections were stained with hematoxylin and eosin, picrosirius red or cytokeratin-19 (CK19, ab52625; Abcam, Cambridge, United Kingdom) according to standard protocols. Images were obtained using a Hamamatsu NanoZoomer (Hamamatsu Photonics, Almere, the Netherlands).

Flow Cytometry

EDTA blood samples from mice were collected and after red blood cell lysis incubated with Fc Block and labeled with conjugated antibodies. Immune cells were isolated from mouse liver by digestion for 30 minutes at 37°C with collagenase D, and subsequent centrifugation with 35% Percoll. Cells were treated with Zombie UV to discriminate live and dead cells. Cells from liver and blood were incubated with Fc Block and labeled with conjugated antibodies: TCRβ (BUV395), CD4 (BUV737), CD8a (BV510), CD3 (BV785), CD11b (FITC), F4/80 (PE-CY5), B220 (PE), CD45 (PE-Texas Red), CD19 (APC), TCR$\gamma\delta$ (APC-CY7). For myeloid cell staining, an additional panel was used with the following antibodies: CD45.2 (BUV737), B220 (BV421), CD11b (BV605), Ly6C (BV785), CD115 (FITC), CLEC4F (PE-CY7), F4/80 (PE-CY5), CCR2 (PE), CD19, CD3, NK1.1 (PE-Texas Red), MHCII (AF700), CD11c (APC-CY7). The Abcam Antibody Coupling Kit (ab102903) was used to couple the CLEC4F antibody to PE-CY7. Flow cytometry analysis was performed on a BD LSR Fortessa X-20 (Becton Dickinson, Franklin Lakes, New Jersey). Results were acquired with the Diva software (v7.0, Becton Dickinson) and analyzed using FlowJo software (v10.6.1, Tree Star, Ashland, OR).

Microbiota Analysis

Composition of the microbiota was analyzed by sequencing of 16S ribosomal DNA, isolated from cecal contents of male mice sacrificed at the age of 12 weeks, on a Illumina HiSeq platform (Novogene, Hong Kong, China), essentially as described.[48] Operational taxonomic units abundance (97% similarity) information was normalized using a standard number of sequences corresponding to the sample with the least reads (<60,000). Subsequent analyses were performed based the normalized data. Taxonomic differences between the groups were determined at the genus level after removal of unidentified and very low-abundant genera, leaving 115 genera for analysis. To compare the overall microbial communities between mice, the unweighted UniFrac distance was calculated based on the taxonomic tree at the genus level using the Phyloseq[49] package for R software (v3.6.1, R Foundation for Statistical Computing, Vienna, Austria) and visualized using principal coordinates analysis. Significance of differences between groups was assessed by the nonparametric Wilcoxon test. The *P* value was adjusted for multiple comparisons using the Benjamini-Hochberg procedure[50] with the FDR set at 5%.

Measurement of Metabolic Fluxes Using Stable Isotopes

Fractional cholesterol absorption was measured following intravenous administration of cholesterol-D_5 and oral administration of cholesterol-D_7.[51] DNL and cholesterol synthesis rates were measured following addition of [1-^{13}C] acetate to the drinking water of the mice and calculated as described.[52] CA kinetics were determined following intravenous administration of 400 μg [24-^{13}C]-CA, essentially as described previously.[53] Total BA pool size was calculated by dividing CA pool size by the fractional abundance of CA in the total BA pool.

Hepatic Lipid Measurements

Livers were homogenized (15%, w/w) in PBS and lipids were extracted according to Bligh and Dyer.[54] Cholesterol and triglycerides were subsequently measured using commercially available reagents (DiaSys Diagnostic Systems and Roche Diagnostics), whereas phospholipids were quantified as described.[39]

Statistics

Data in graphs are presented as bar graphs with SEM, Tukey box-and-whisker plots or line graphs with median and interquartile range. Statistical analyses between 2 groups were performed by Mann-Whitney *U* nonparametric comparisons (GraphPad Software, San Diego, CA), whereas the Kruskal-Wallis H test followed by Conover post hoc analysis (Brightstat)[55] was used for multiple group comparisons. Differences were considered statistically significant when *P* values were <.05.

References

1. Moschetta A, Xu F, Hagey LR, van Berge-Henegouwen GP, van Erpecum KJ, Brouwers JF, Cohen JC, Bierman M, Hobbs HH, Steinbach JH, Hofmann AF. A phylogenetic survey of biliary lipids in vertebrates. J Lipid Res 2005;46:2221–2232.
2. Kuipers F, Bloks VW, Groen AK. Beyond intestinal soap-bile acids in metabolic control. Nat Rev Endocrinol 2014; 10:488–498.
3. de Boer JF, Bloks VW, Verkade E, Heiner-Fokkema MR, Kuipers F. New insights in the multiple roles of bile acids and their signaling pathways in metabolic control. Curr Opin Lipidol 2018;29:194–202.
4. Takahashi S, Fukami T, Masuo Y, Brocker CN, Xie C, Krausz KW, Wolf CR, Henderson CJ, Gonzalez FJ. Cyp2c70 is responsible for the species difference in bile acid metabolism between mice and humans. J Lipid Res 2016;57:2130–2137.
5. De Boer JF, Verkade E, Mulder NL, De Vries HD, Huijkman N, Koehorst M, Boer T, Wolters JC, Bloks VW, Van De Sluis B, Kuipers F. A human-like bile acid pool induced by deletion of hepatic Cyp2c70 modulates effects of FXR activation in mice. J Lipid Res 2020; 61:291–305.
6. Honda A, Miyazaki T, Iwamoto J, Hirayama T, Morishita Y, Monma T, Ueda H, Mizuno S, Sugiyama F, Takahashi S, Ikegami T. Regulation of bile acid metabolism in mouse models with hydrophobic bile acid composition. J Lipid Res 2020;61:54–69.
7. Straniero S, Laskar A, Savva C, H Aumlrdfeldt J, Angelin B, Rudling M. Of mice and men: Murine bile acids explain species differences in the regulation of bile acid and cholesterol metabolism. J Lipid Res 2020; 61:480–491.
8. Chiang JYL, Ferrell JM. Bile acid metabolism in liver pathobiology. Gene Expr 2018;18:71–87.
9. Jansen PLM, Ghallab A, Vartak N, Reif R, Schaap FG, Hampe J, Hengstler JG. The ascending pathophysiology of cholestatic liver disease. Hepatology 2017; 65:722–738.
10. Heuman DM. Quantitative estimation of the hydrophilic-hydrophobic balance of mixed bile salt solutions. J Lipid Res 1989;30:719–730.
11. Kitani K, Kanai S, Sato Y, Ohta M. Tauro alpha-muricholate is as iffective as tauro beta-muricholate and tauroursodeoxycholate in preventing taurochenodeoxycholate-induced liver damage in the rat. Hepatology 1994;19:1007–1012.
12. Fuchs CD, Traussnigg SA, Trauner M. Nuclear receptor modulation for the treatment of nonalcoholic fatty liver disease. Semin Liver Dis 2016;36:69–86.
13. Pols TWH, Noriega LG, Nomura M, Auwerx J, Schoonjans K. The bile acid membrane receptor TGR5: A valuable metabolic target. Dig Dis 2011;29:37–44.
14. Gerussi A, D'Amato D, Cristoferi L, O'Donnell SE, Carbone M, Invernizzi P. Multiple therapeutic targets in rare cholestatic liver diseases: Time to redefine treatment strategies. Ann Hepatol 2020;19:5–16.
15. Porez G, Prawitt J, Gross B, Staels B. Bile acid receptors as targets for the treatment of dyslipidemia and cardiovascular disease. J Lipid Res 2012;53:1723–1737.
16. Parks DJ, Blanchard SG, Bledsoe RK, Chandra G, Consler TG, Kliewer SA, Stimmel JB, Willson TM, Zavacki AM, Moore DD, Lehmann JM. Bile acids: natural ligands for an orphan nuclear receptor. Science 1999; 284:1365–1368.
17. Sayin SI, Wahlström A, Felin J, Jäntti S, Marschall H-U, Bamberg K, Angelin B, Hyötyläinen T, Orešič M, Bäckhed F. Gut microbiota regulates bile acid metabolism by reducing the levels of tauro-beta-muricholic acid, a naturally occurring FXR antagonist. Cell Metab 2013;17:225–235.
18. Maruyama T, Miyamoto Y, Nakamura T, Tamai Y, Okada H, Sugiyama E, Nakamura T, Itadani H, Tanaka K. Identification of membrane-type receptor for bile acids (M-BAR). Biochem Biophys Res Commun 2002; 298:714–719.
19. Guo GL, Chiang JYL. Is CYP2C70 the key to new mouse models to understand bile acids in humans? J Lipid Res 2020;61:269–271.
20. Boonstra K, Beuers U, Ponsioen CY. Epidemiology of primary sclerosing cholangitis and primary biliary cirrhosis: A systematic review. J Hepatol 2012; 56:1181–1188.
21. Lonardo A, Nascimbeni F, Ballestri S, Fairweather DL, Win S, Than TA, Abdelmalek MF, Suzuki A. Sex differences in nonalcoholic fatty liver disease: state of the art and identification of research gaps. Hepatology 2019; 70:1457–1469.
22. Oude Elferink RPJ. Cholestasis. Gut 2003;52:ii42–ii48.
23. Gurantz D, Hofmann AF. Influence of bile acid structure on bile flow and biliary lipid secretion in the hamster. Am J Physiol Liver Physiol 1984;247:G736–G748.
24. Ridlon JM, Kang DJ, Hylemon PB, Bajaj JS. Bile acids and the gut microbiome. Curr Opin Gastroenterol 2014; 30:332–338.
25. Parkar SG, Kalsbeek A, Cheeseman JF. Potential role for the gut microbiota in modulating host circadian rhythms and metabolic health. Microorganisms 2019;7:41.
26. Özcan U, Yilmaz E, Özcan L, Furuhashi M, Vaillancourt E, Smith RO, Görgün CZ, Hotamisligil GS. Chemical chaperones reduce ER stress and restore glucose homeostasis in a mouse model of type 2 diabetes. Science 2006;313:1137–1140.
27. Ashby K, Navarro Almario EE, Tong W, Borlak J, Mehta R, Chen M. Review article: therapeutic bile acids and the risks for hepatotoxicity. Aliment Pharmacol Ther 2018;47:1623–1638.

28. Scheer N, Kapelyukh Y, Chatham L, Rode A, Buechel S, Wolf CR. Generation and characterization of novel cytochrome P450 Cyp2c gene cluster knockout and CYP2C9 humanized mouse lines. Mol Pharmacol 2012; 82:1022–1029.
29. Koopen N, Post S, Wolters H, Havinga R, Stellaard F, Boverhof R, Kuipers F, Princen H. Differential effects of 17alpha-ethinylestradiol on the neutral and acidic pathways of bile salt synthesis in the rat. J Lipid Res 1999; 40:100–108.
30. Renaud HJ, Cui JY, Khan M, Klaassen CD. Tissue distribution and gender-divergent expression of 78 cytochrome P450 mRNAs in mice. Toxicol Sci 2011; 124:261–277.
31. Wang DQH, Tazuma S, Cohen DE, Carey MC. Feeding natural hydrophilic bile acids inhibits intestinal cholesterol absorption: Studies in the gallstone-susceptible mouse. Am J Physiol - Gastrointest Liver Physiol 2003; 285:G494–G502.
32. Tang WHW, Bäckhed F, Landmesser U, Hazen SL. Intestinal microbiota in cardiovascular health and disease: JACC State-of-the-Art Review. J Am Coll Cardiol 2019; 73:2089–2105.
33. Chen W, Wei Y, Xiong A, Li Y, Guan H, Wang Q, Miao Q, Bian Z, Xiao X, Lian M, Zhang J, Li B, Cao Q, Fan Z, Zhang W, Qiu D, Fang J, Gershwin ME, Yang L, Tang R, Ma X. Comprehensive analysis of serum and fecal bile acid profiles and interaction with gut microbiota in primary biliary cholangitis. Clin Rev Allergy Immunol 2020; 58:25–38.
34. Ottman N, Geerlings SY, Aalvink S, de Vos WM, Belzer C. Action and function of Akkermansia muciniphila in microbiome ecology, health and disease. Best Pract Res Clin Gastroenterol 2017;31:637–642.
35. Zöhrer E, Resch B, Scharnagl H, Schlagenhauf A, Fauler G, Stojakovic T, Hofer N, Lang U, Jahnel J. Serum bile acids in term and preterm neonates: A case-control study determining reference values and the influence of early-onset sepsis. Medicine 2016;95:e5219.
36. Poirier S, Mamarbachi M, Chen W-T, Lee AS, Mayer G. GRP94 regulates circulating cholesterol levels through blockade of PCSK9-induced LDLR degradation. Cell Rep 2015;13:2064–2071.
37. Schonewille M, de Boer JF, Mele L, Wolters H, Bloks VW, Wolters JC, Kuivenhoven JA, Tietge UJF, Brufau G, Groen AK. Statins increase hepatic cholesterol synthesis and stimulate fecal cholesterol elimination in mice. J Lipid Res 2016;57:1455–1464.
38. Rimbert A, Dalila N, Wolters JC, Huijkman N, Smit M, Kloosterhuis N, Riemsma M, Van Der Veen Y, Singla A, Van Dijk F, Frikke-Schmidt R, Burstein E, Tybjærg-Hansen A, Van De Sluis B, Kuivenhoven JA. A common variant in CCDC93 protects against myocardial infarction and cardiovascular mortality by regulating endosomal trafficking of low-density lipoprotein receptor. Eur Heart J 2020;41:1040–1053.
39. Böttcher CJF, Van gent CM, Pries C. A rapid and sensitive sub-micro phosphorus determination. Anal Chim Acta 1961;24:203–204.
40. Paumelle R, Haas JT, Hennuyer N, Baugé E, Deleye Y, Mesotten D, Langouche L, Vanhoutte J, Cudejko C, Wouters K, Hannou SA, Legry V, Lancel S, Lalloyer F, Polizzi A, Smati S, Gourdy P, Vallez E, Bouchaert E, Derudas B, Dehondt H, Gheeraert C, Fleury S, Tailleux A, Montagner A, Wahli W, Van Den Berghe G, Guillou H, Dombrowicz D, Staels B. Hepatic PPARα is critical in the metabolic adaptation to sepsis. J Hepatol 2019; 70:963–973.
41. Lin K, Kools H, de Groot P, Gavai A, Basnet R, Cheng F, Wu J, Wang X, Lommen A, Hooiveld G, Bonnema G, Visser R, Muller M, Leunissen J. MADMAX - Management and analysis database for multiple ~omics experiments. J Integr Bioinform 2011;8:160.
42. Sartor MA, Tomlinson CR, Wesselkamper SC, Sivaganesan S, Leikauf GD, Medvedovic M. Intensity-based hierarchical Bayes method improves testing for differentially expressed genes in microarray experiments. BMC Bioinformatics 2006;7:538.
43. Subramanian A, Tamayo P, Mootha VK, Mukherjee S, Ebert BL, Gillette MA, Paulovich A, Pomeroy SL, Golub TR, Lander ES, Mesirov JP. Gene set enrichment analysis: A knowledge-based approach for interpreting genome-wide expression profiles. Proc Natl Acad Sci U S A 2005;102:15545–15550.
44. Gentleman RC, Carey VJ, Bates DM, Bolstad B, Dettling M, Dudoit S, Ellis B, Gautier L, Ge Y, Gentry J, Hornik K, Hothorn T, Huber W, Iacus S, Irizarry R, Leisch F, Li C, Maechler M, Rossini AJ, Sawitzki G, Smith C, Smyth G, Tierney L, Yang JYH, Zhang J. Bioconductor: open software development for computational biology and bioinformatics. Genome Biol 2004;5:R80.
45. Carvalho BS, Irizarry RA. A framework for oligonucleotide microarray preprocessing. Bioinformatics 2010; 26:2363–2367.
46. Ritchie ME, Phipson B, Wu D, Hu Y, Law CW, Shi W, Smyth GK. Limma powers differential expression analyses for RNA-sequencing and microarray studies. Nucleic Acids Res 2015;43:e47.
47. van der Laan MJ, Pollard KS. A new algorithm for hybrid hierarchical clustering with visualization and the bootstrap. J Stat Plan Inference 2003;117:275–303.
48. Brandsma E, Kloosterhuis NJ, Koster M, Dekker DC, Gijbels MJJ, van der Velden S, Ríos-Morales M, van Faassen MJR, Loreti MG, de Bruin A, Fu J, Kuipers F, Bakker BM, Westerterp M, de Winther MPJ, Hofker MH, van de Sluis B, Koonen DPY. A proinflammatory gut microbiota increases systemic inflammation and accelerates atherosclerosis. Circ Res 2019;124:94–100.
49. McMurdie PJ, Holmes S. Phyloseq: An R package for reproducible interactive analysis and graphics of microbiome census data. PLoS One 2013;8:e61217.
50. Benjamini Y, Hochberg Y. Controlling the false discovery rate: A practical and powerful approach to multiple testing. J R Stat Soc Ser B 1995;57:289–300.
51. Brufau G, Kuipers F, Lin Y, Trautwein EA, Groen AK. A reappraisal of the mechanism by which plant sterols promote neutral sterol loss in mice. PLoS One 2011;6: e21576.

52. van der Veen JN, van Dijk TH, Vrins CLJ, van Meer H, Havinga R, Bijsterveld K, Tietge UJF, Groen AK, Kuipers F. Activation of the liver X receptor stimulates trans-intestinal excretion of plasma cholesterol. J Biol Chem 2009;284:19211–19219.
53. Stellaard F, Sackmann M, Sauerbruch T, Paumgartner G. Simultaneous determination of cholic acid and chenodeoxycholic acid pool sizes and fractional turnover rates in human serum using 13C-labeled bile acids. J Lipid Res 1984;25:1313–1319.
54. Bligh EG, Dyer WJ. A rapid method of total lipid extraction and purification. Can J Biochem Physiol 1959; 37:911–917.
55. Stricker D. BrightStat.com: free statistics online. Comput Methods Programs Biomed 2008;92:135–143.

Received September 8, 2020. Accepted December 4, 2020.

Correspondence
Address correspondence to: Jan Freark de Boer, PhD, University Medical Center Groningen, Department of Pediatrics, Hanzeplein 1, 9713 GZ, Groningen, the Netherlands. e-mail: j.f.de.boer@umcg.nl; fax: +31(0)503611746.

Acknowledgments
Hilde D. de Vries, Anna Palmiotti, and Rumei Li contributed equally to this study.

The authors thank Marieke Smit, Rick Havinga, Ingrid Martini, Venetia Bazioti, Valentine Guinot, and Laurent Pineau for their expert assistance during the experiments.

CRediT Authorship Contributions

Jan Freark de Boer, PhD (Conceptualization: Equal; Data curation: Equal; Formal analysis: Equal; Funding acquisition: Equal; Investigation: Lead; Supervision: Equal; Writing – review & editing: Equal)

Hilde D. de Vries, MSc (Data curation: Equal; Formal analysis: Equal; Writing – original draft: Equal)

Anna Palmiotti, MSc (Data curation: Equal; Formal analysis: Equal; Writing – original draft: Equal)

Rumei Li, MSc (Data curation: Equal; Formal analysis: Equal; Writing – original draft: Equal)

Marwah Doestzada, MSc (Formal analysis: Equal)

Joanne A. Hoogerland, MSc (Data curation: Equal; Formal analysis: Equal; Writing – review & editing: Equal)

Jingyuan Fu, PhD (Formal analysis: Equal; Writing – review & editing: Equal)

Anouk M. La Rose, MSc (Data curation: Equal; Formal analysis: Equal)

Marit Westerterp, PhD (Formal analysis: Equal; Writing – review & editing: Equal)

Niels L Mulder, BSc (Data curation: Equal)

Milaine V. Hovingh, BSc (Data curation: Equal)

Martijn Koehorst, BSc (Data curation: Equal)

Niels J Kloosterhuis, BSc (Data curation: Equal)

Justina C. Wolters, PhD (Data curation: Equal)

Vincent W. Bloks, BSc (Conceptualization: Equal; Formal analysis: Equal; Writing – review & editing: Equal)

Joel T. Haas, PhD (Data curation: Equal; Formal analysis: Equal; Writing – review & editing: Equal)

David Dombrowicz, PhD (Formal analysis: Equal; Writing – review & editing: Equal)

Bart Staels, PhD (Writing – review & editing: Equal)

Bart van de Sluis, PhD (Formal analysis: Equal; Writing – review & editing: Equal)

Folkert Kuipers, PhD (Conceptualization: Equal; Funding acquisition: Equal; Supervision: Equal; Writing – review & editing: Equal)

Conflicts of Interest
The authors disclose no conflicts.

Funding
Jan Freark de Boer is supported by the Nutrition and Health initiative of the University of Groningen. Anna Palmiotti is supported by the European Union's Horizon 2020 research and innovation program under the Marie Skłodowska-Curie grant agreement no. 754425. Rumei Li is supported by China Scholarship Council (no. 201806100216). Jingyuan Fu is funded by a Netherlands Organization for Scientific Research (NWO) VIDI grant (864.13.013), the Netherlands Heart Foundation (IN CONTROL, CVON2018-27), and the NWO Netherlands Organ-on-Chip Initiative (024.003.001). Marit Westerterp is funded by an NWO VIDI grant (917.15.350) and a Rosalind Franklin Fellowship from the University Medical Center Groningen. Bart Staels is supported by grants from the European Genomic Institute for Diabetes (EGID, ANR-10-LABX-46) and Agence Nationale pour la Recherche (ANR-FXREn), and holds a European Research Council advanced grant (694717). Folkert Kuipers is supported by the Netherlands Heart Foundation (IN CONTROL, CVON2018-27) and the Noaber Foundation (Lunteren, the Netherlands).